



Groundwater noble gas, age, and temperature signatures in an Alpine watershed: Valuable tools in conceptual model development

Andrew H. Manning¹ and Jonathan Saul Caine¹

Received 19 July 2006; revised 7 November 2006; accepted 22 November 2006; published 4 April 2007.

[1] Bedrock groundwater in alpine watersheds is poorly understood, mainly because of a scarcity of wells in alpine settings. Groundwater noble gas, age, and temperature data were collected from springs and wells with depths of 3–342 m in Handcart Gulch, an alpine watershed in Colorado. Temperature profiles indicate active groundwater circulation to a maximum depth (aquifer thickness) of about 200 m, or about 150 m below the water table. Dissolved noble gas data show unusually high excess air concentrations ($>0.02 \text{ cm}^3 \text{ STP/g}$, $\Delta\text{Ne} > 170\%$) in the bedrock, consistent with unusually large seasonal water table fluctuations (up to 50 m) observed in the upper part of the watershed. Apparent $^3\text{H}/^3\text{He}$ ages are positively correlated with sample depth and excess air concentrations. Integrated samples were collected from artesian bedrock wells near the trunk stream and are assumed to approximate flow-weighted samples reflecting bedrock aquifer mean residence times. Exponential mean ages for these integrated samples are remarkably consistent along the stream, four of five being from 8 to 11 years. The tracer data in combination with other hydrologic and geologic data support a relatively simple conceptual model of groundwater flow in the watershed in which (1) permeability is primarily a function of depth; (2) water table fluctuations increase with distance from the stream; and (3) recharge, aquifer thickness, and porosity are relatively uniform throughout the watershed in spite of the geological complexity of the Proterozoic crystalline rocks that underlie it.

Citation: Manning, A. H., and J. S. Caine (2007), Groundwater noble gas, age, and temperature signatures in an Alpine watershed: Valuable tools in conceptual model development, *Water Resour. Res.*, 43, W04404, doi:10.1029/2006WR005349.

1. Introduction

[2] A growing number of studies indicate that groundwater with an age ≥ 1 year can be a significant component of the hydrologic system in headwater catchments, including high-elevation alpine catchments that have limited soil cover and are at least partly above tree line [e.g., Liu *et al.*, 2004; Sueker *et al.*, 2000; Uhlenbrook *et al.*, 2002; Soulsby *et al.*, 2000; Mau and Winter, 1997; Herrmann and Stichler, 1980; Bossong *et al.*, 2003]. Several of these studies identify bedrock groundwater, specifically, as an important contributor (20–50%) to annual surface water discharge [Uhlenbrook *et al.*, 2002; Kosugi *et al.*, 2006; Tiedeman *et al.*, 1998; Bossong *et al.*, 2003; Mulholland, 1993]. These studies imply that bedrock groundwater potentially exerts a major influence on surface water chemistry in mountain watersheds, and some studies have in fact observed this influence [Kimball *et al.*, 2001, 2002; Burns *et al.*, 1998]. Economies in mountain regions often directly rely upon the chemistry and quality of mountain surface waters [e.g., Todd and McKnight, 2003]. Aside from its potential influence on surface water, mountain bedrock groundwater is itself an important resource because of its increasing direct utilization by growing mountain communities [Bossong *et*

al., 2003; Caine and Tomusiak, 2003], and its role in recharging adjacent basin aquifers as “mountain-block recharge” in some regions [Wilson and Guan, 2004; Manning and Solomon, 2005].

[3] However, mountain and alpine bedrock aquifers are poorly understood. They are potentially highly complex systems, commonly involving structurally complicated rocks, extreme head gradients (ground slope angles 10° – 40°), and dramatically fluctuating recharge due to seasonal snowmelt. Head data are rare, particularly from upper portions of watersheds. Studies attempting to characterize mountain aquifers are limited (especially for alpine settings), and rely largely on lumped parameter modeling [e.g., Maloszewski *et al.*, 1983; Uhlenbrook *et al.*, 2002], streamflow recession modeling [e.g., Mendoza *et al.*, 2003; Zecharias and Brutsaert, 1988], and environmental tracer data collected from springs and tunnels [e.g., Rademacher *et al.*, 2001, 2003; Maréchal and Etcheverry, 2003]. Lumped parameter and streamflow recession modeling provide single aquifer parameter values for the entire watershed, and no information on the degree to which they might vary spatially. Further, aquifer parameters determined from recession modeling are inherently nonunique because the derived parameter is actually aquifer diffusivity, a combined parameter that is a function of aquifer thickness, hydraulic conductivity, and storage. Springs provide only a limited window into the groundwater system; flow pathways leading to a spring are seldom known with any confidence, so

¹U.S. Geological Survey, Denver, Colorado, USA.

the depth intervals represented in a spring sample are generally unknown. Tunnels provide direct access to different depths within the flow system, but they can severely perturb natural flow paths and rates, drawing near-surface water to depths well below where it normally circulates [Polyakov *et al.*, 1996]. Few watershed-scale numerical groundwater flow models have been constructed [Tiedeman *et al.*, 1998; VanderBeek, 2003], and the lack of wells located in upper portions of the watershed and/or that penetrate to depths below the aquifer raise questions about assumed basal boundary conditions and derived hydraulic conductivity values.

[4] A need clearly exists for strategically located wells in an alpine watershed that allow direct observation of the groundwater at different depths. The Handcart Gulch Study site in the Colorado Front Range was developed by the U.S. Geological Survey (USGS) to address this research need, with an emphasis on better understanding solute transport processes in mountain groundwater systems that naturally generate acid rock drainage [Caine *et al.*, 2006]. Wells with depths ranging from 3 to 342 m were installed along the trunk stream and in upper parts of the watershed, the highest well being located directly on the Continental Divide at 3688 m above sea level (asl). This paper presents groundwater temperature, age, and dissolved gas data collected from both wells and springs at the site. The data address four fundamental questions about alpine groundwater flow systems in fractured crystalline bedrock: (1) What is the depth to which groundwater actively circulates, and how much does that depth vary throughout the watershed? (2) What is the mean residence time of groundwater in the watershed, and how does it vary between different sections of the watershed in response to spatial variations in recharge rate, porosity, and aquifer thickness? (3) What are characteristic dissolved noble gas signatures, and do they provide useful information about recharge dynamics? (4) Is modeling watershed-scale groundwater flow with an equivalent porous media model justifiable using data from a limited number of wells, or is the system too heterogeneous on a watershed scale? The tracer data play an important role in the development of a defensible conceptual model of the groundwater flow system, without which any future numerical modeling would be of limited value.

2. Approach

[5] One objective of research in Handcart Gulch is to build a numerical coupled heat and fluid flow model of the watershed that will provide insights into processes controlling the natural generation and transport of acidic and metal-rich waters. In order to do so, a reasonably well supported conceptual model is required. A host of other data types were collected from the site in addition to the data presented in this paper, including head measurements, aquifer tests, core logging, outcrop mapping, borehole geophysical logging, etc. [Caine *et al.*, 2006]. These data suggest that the groundwater flow system has the following basic characteristics: (1) Groundwater flow occurs in bedrock and overlying surficial materials; (2) the bedrock, consisting of complexly fractured crystalline metamorphic rocks, has sufficient hydraulic conductivity ($>10^{-8}$ m/s) to transmit a substantial fraction of precipitation, given observed head gradients of about 0.2; (3) heads generally mimic topogra-

phy, meaning that groundwater flow is directed toward the trunk stream, which gains throughout the site; (4) the groundwater system is highly dynamic, with seasonal head variations of up to 50 m in upper portions of the watershed; and (5) bedrock permeability is primarily a function of depth rather than being controlled by a few discrete geologic structures, given that the bedrock is pervasively fractured and few individual water-bearing fractures could be identified in boreholes. In this paper, permeability and hydraulic conductivity refer to the bulk permeability and bulk hydraulic conductivity, applicable to a watershed scale flow model. Two important characteristics of the flow system not addressed by these data include (1) the depth to which groundwater flow actively occurs (aquifer thickness); and (2) the degree to which aquifer thickness, recharge rate (probably controlled in part by permeability), and porosity vary throughout the watershed. The latter is particularly uncertain given the limited well coverage and the fact that groundwater flow in fractured crystalline rocks can be highly heterogeneous and complex at a variety of scales. Note that by aquifer thickness we do not mean the depth to a discrete, well-defined aquifer bottom, but instead the depth to some level within a continuum of decreasing permeability below which relatively little groundwater flow occurs.

[6] The concept that bedrock groundwater flow in mountains dominantly occurs in a shallow higher-permeability zone ("active" or "decompressed" zone) that overlies a deeper lower-permeability zone hosting little flow ("inactive" or "passive" zone) has been described by several workers [e.g., Snow, 1973; Robinson *et al.*, 1974; Maréchal, 1999; Caine and Tomusiak, 2003; Mayo *et al.*, 2003]. We prefer the terms "active" and "inactive," and will use these henceforth. It is important to understand, however, that some amount of flow does occur in the inactive zone and can be significant on a geologic timescale. Higher permeability at shallower depths is generally attributed to a greater degree of weathering and/or smaller overburden loads allowing more fractures to remain open.

[7] Active and inactive zones have been delineated using multiple approaches, including (1) groundwater ages determined from environmental tracers [e.g., Mayo *et al.*, 2003; Maréchal and Etcheverry, 2003]; (2) discrete-interval aquifer tests, fracture observations, and production information from wells [e.g., Dekay, 1972; Rahn, 1981]; (3) tunnel inflow observations [e.g., Desbarats, 2002; Mayo *et al.*, 2003]; (4) temperature data, mainly from tunnels within the inactive zone [e.g., Robinson, 1978; Mayo and Koontz, 2000]; and (5) seismic velocity contrasts [Robinson *et al.*, 1974]. In this study we employ temperature data but move beyond previous applications by measuring temperature profiles from borings that transect the active zone and penetrate into the inactive zone below.

[8] Because ground temperatures are sensitive to groundwater flow rates, temperature profiles serve as a direct and continuous measure of the change in flow rate with depth in a mountain mass. The transition between linear temperature profiles with gradients similar to the local conductive geothermal gradient (conductive profiles) and nonlinear temperature profiles associated with advective heat transport from groundwater flow (disturbed profiles) is associated with Peclet numbers in the 0.1–0.4 range [Bredehoeft

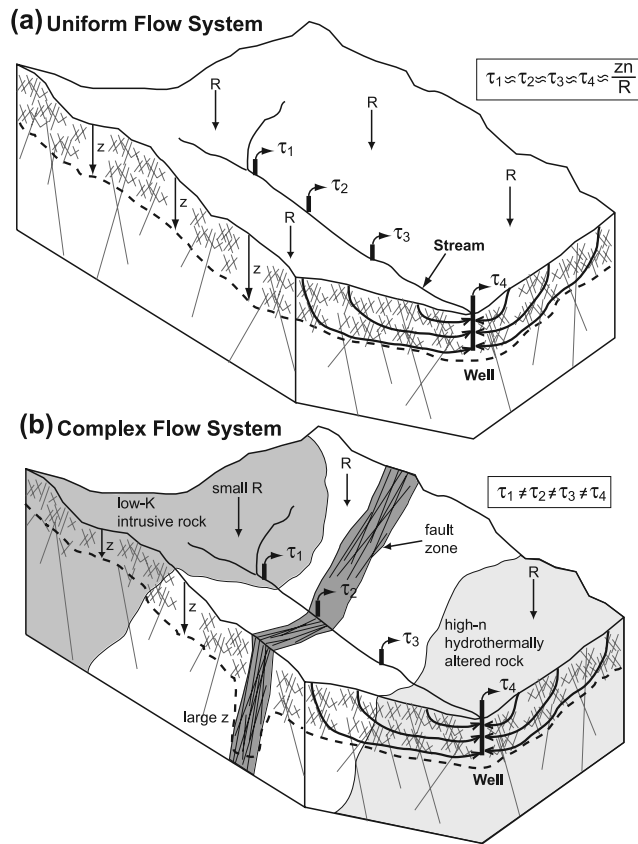


Figure 1. Schematic diagrams illustrating two different conceptual models of groundwater flow in an alpine watershed underlain by fractured crystalline rock. (a) Uniform flow system in which aquifer thickness (z), recharge rate (R), and porosity (n) are relatively uniform throughout the watershed. Mean residence times (τ) from samples from wells along the creek that integrate all flow paths to the creek (flow-weighted samples) are uniform and equal to zn/R [Haitjema, 1995]. (b) Complex flow system in which z , R , and n vary throughout the watershed, resulting in variations in τ along the creek.

and Papadopulos, 1965; Ferguson et al., 2006]. Simple calculations performed using Peclet number definitions by Bredehoeft and Papadopulos [1965] and Domenico and Palciauskas [1973], and assuming reasonable parameters for an alpine bedrock aquifer, indicate that conductive profiles can only be maintained in such aquifers if vertical groundwater Darcy flow velocities are of the order of centimeters per year or less. These calculations do not take into account the pronounced decrease in mean annual surface ground temperature with elevation expected in mountain settings. Conductive profiles in these settings therefore probably indicate maximum vertical flow velocities closer to 1 cm/yr than 10 cm/yr. This is supported by numerical modeling of heat and fluid transport in mountainous terrain performed by Forster and Smith [1989] indicating that disturbance of the conductive geotherm occurs at infiltration rates greater than about 1 cm/yr. Because estimated recharge rates in alpine watersheds are typically tens of centimeters per year [e.g., Hely et al., 1971; Wasiolek, 1995; Guan, 2005] and topographic gradients are generally steep, vertical flow velocities in the active zone

generally should be high enough to result in disturbed profiles. Further, conductive profiles typically should indicate vertical flow rates $<10\%$ of the recharge rate. We believe that flow rates on this scale constitute a sensible definition of the inactive zone, and therefore we use temperature profiles to distinguish active from inactive zones in this study. One concern with this approach is that boreholes can disturb the natural groundwater flow system by connecting previously unconnected zones of permeability and enhancing vertical groundwater flow. However, these disturbances are likely to be considerably smaller than those caused by tunnels, and at worst this approach provides a robust maximum depth for the bottom of the active zone.

[9] Haitjema [1995] demonstrated that the mean age of groundwater discharging to a stream should be constant throughout a watershed if aquifer thickness (z), recharge rate (R), and porosity (n) are constant throughout that watershed. Haitjema's [1995] work is essentially a three-dimensional extension of the classical two-dimensional exponential flow model [Vogel, 1967; Maloszewski and Zuber, 1982; Cook and Böhlke, 2000], a lumped-parameter model in which the age distribution of discharging groundwater has an exponential form (exponentially more young water than old water). The results of Haitjema [1995] present a method for evaluating the assumption that z , R , and n are relatively constant throughout a watershed. If these parameters are indeed constant, and if groundwater samples can be collected at multiple locations along a stream such that each sample integrates all groundwater discharging to the stream at that location (flow-weighted sample), then the mean age of these different flow-weighted samples should be constant. Conversely, if z , R , and n vary significantly on a watershed scale due to major fault zones intersecting the stream, lithologic changes, and so forth, then the mean age of flow-weighted samples should also vary significantly (Figure 1). Henceforth the former case shall be referred to as a "uniform flow system" (Figure 1a) and latter case shall be referred to as a "complex flow system" (Figure 1b). It is important to understand that in alpine fractured crystalline rock aquifers, recharge is probably permeability-limited because permeabilities are relatively low and recharge occurs in large seasonal bursts due to spring snowmelt. This means that significant watershed scale variations in permeability (other than depth-dependent) should also result in variations in the mean age of flow-weighted samples. Note that groundwater flow may be largely parallel to the two tributaries in the uppermost part of the watershed shown in Figure 1 (rather than perpendicular to them, as with the trunk stream) if they have gradients similar to the topographic gradients of surrounding slopes (as is the case in Handcart Gulch).

[10] Observing uniform mean ages of flow-weighted samples along a stream of course does not prove the presence of a uniform flow system because it is possible that effects of variations in these parameters could happen to cancel each other out. Furthermore, such uniform ages could also occur if these parameters varied uniformly with depth or with distance from the stream (for example, if R increased with elevation, which uniformly increased with distance from the stream). Nonetheless, such uniform mean ages would still serve as supporting evidence that these parameters are either relatively constant or vary in a

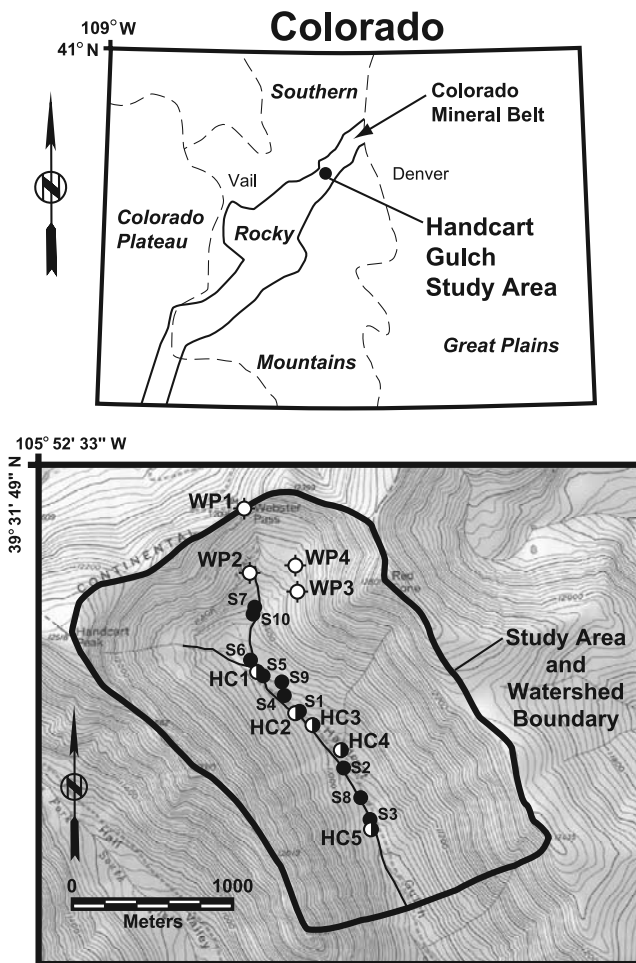


Figure 2. Location of Handcart Gulch study area, deep wells (WP1–WP4), well clusters near trunk stream (HC1–HC5), and springs (S1–S10).

systematic way on a watershed scale, and that a relatively simple equivalent porous media model might represent the groundwater flow system sufficiently well to provide useful information about watershed-scale flow and transport processes.

[11] Collecting a true flow-weighted sample poses a significant sampling challenge and actually may be nearly impossible. However, the fact that alpine fractured rock aquifers generally have low permeabilities and steep hydraulic gradients means that pronounced upward gradients should exist under the trunk stream. Wells installed in the bedrock under the stream to even a modest depth should therefore produce artesian flow and thus serve as a drain that intercepts groundwater flow paths that otherwise would have flowed to the stream. This artesian flow should provide a good approximation of a flow-weighted sample. This subject is discussed further in section 4.

3. Site Description

[12] Handcart Gulch is a 4.7-km² alpine watershed located in the Colorado Rocky Mountain Front Range (Figure 2). Elevations range from 3300 to 3900 m asl. Meteorological stations in the area (none is located in Handcart Gulch)

suggest that average annual precipitation is about 85 cm, and about 65% of this falls as snow. Vegetation is subalpine to alpine, dominantly mixed spruce and fir forest, or tundra. The stream draining the watershed is perennial, and monthly average stream discharge ranges from about 3 L/s to about 120 L/s [Kahn, 2005]. A tracer dilution study performed in the summer of 2003 indicates that the stream gains continually throughout the site [Runkel *et al.*, 2003].

[13] Handcart Gulch is located in the southeastern portion of the Montezuma mining district of the Colorado Mineral Belt (Figure 2). The stream draining Handcart Gulch is naturally acidic (pH 2.6–4.6) with elevated metal concentrations due to the presence of a small, unmined, porphyry-related deposit that consists primarily of pyrite. The deposit lies within complexly fractured and tightly folded Precambrian metavolcanic and metasedimentary bedrock [Lovering, 1935]. Geologic structures include a few brittle, small-displacement (of the order of meters to a few tens of meters) faults and high-intensity joint networks. In addition to various tectonic deformation events of regional scale, intrusion of Tertiary porphyry stocks and dikes caused extensive fracturing spatially associated with pervasive and disseminated hydrothermal alteration that is the source of the pyrite. Along the valley floor, the bed of the trunk stream along most of its course is lined by ferricrete (iron-oxide cemented alluvial and colluvial deposits) that can be over 10 m thick. A rock glacier is present in the northeastern part of the watershed which shows evidence of recent motion.

[14] In the summers of 2001 and 2002, the four deep observation wells located in the upper part of the watershed (WP1–WP4, Figure 2) were originally drilled as mineral exploration boreholes with recovery of full drill cores by a private company. These boreholes are 7.5–10 cm in diameter and range in depth from 480 to 1070 m. They were subsequently donated to the USGS and reconditioned for use as observation wells. Unfortunately, casing could not be installed to the total depth of each borehole due to caved intervals, so total depths of the completed WP wells are 91–342 m [Caine *et al.*, 2006]. WP wells are either screened continuously or open within the bedrock. In the fall of 2003 the WP wells were supplemented with nine new shallow observation wells clustered in five different locations adjacent to the trunk stream (HC1–HC5, Figure 2). HC wells completed exclusively in the bedrock (HCBW1–HCBW4) have total depths of 30–52 m (Table 1), and are henceforth referred to as “bedrock HC wells.” HC wells completed exclusively in overlying colluvium (HCCW3), ferricrete (HCFW3), or both (HCSW1 and HCSW2) have total depths of 3–9 m (Table 1) and are henceforth referred to as “shallow wells.” The single well at HC5 (HCFW5) has a total depth of 7 m and is completed in both the upper 1.5 m of bedrock and overlying materials. Significant artesian flow was encountered during drilling of HCFW5 when the bedrock was penetrated, meaning that the majority of flow from the well is probably from the bedrock. HCFW5 is therefore considered a bedrock HC well in further discussions. All HC wells are continuously screened (Table 1) and are 5 or 6.4 cm in diameter [Caine *et al.*, 2006].

[15] Downhole televiewer data indicate pervasive and high-intensity fracture networks at all depths logged (0–335 m). Downhole flow metering performed in concert with the televiewer logging revealed few discrete features con-

Table 1. Sample Information and Dissolved Gas Concentrations^a

Sample Site	Elevation, m asl	Screen Top, m	Screen Bottom, m	Sample Name	Sample Type	Sample Depth, m	Sample Method	Field Parameters				Dissolved Gas Concentrations					
								T, °C	DO, ppm	TGP, atm	Hc, cm ³ STP/g	Ne, cm ³ STP/g	N ₂ , cm ³ STP/g	Ar, cm ³ STP/g	Kr, cm ³ STP/g		
S1	3378	NA	NA	HCS1	spring	NA	DS	2.2	8.75	0.673	3.32E-08 ^b	1.51E-07	1.20E-02	3.24E-04	8.09E-08		
S2	3331	NA	NA	HCS2	spring	NA	DS	4.8	6.71	0.681	3.10E-08	1.37E-07	1.15E-02	3.14E-04	7.75E-08		
S3	3303	NA	NA	HCS3	spring	NA	DS	12.2	2.93	0.656	3.59E-08	1.56E-07	1.14E-02	2.98E-04	7.14E-08		
S4	3394	NA	NA	HCS4	spring	NA	DS	5.0	0.57	0.727	3.39E-08	1.54E-07	1.48E-02	3.88E-04	9.36E-08		
S5	3413	NA	NA	HCS5	spring	NA	DS	5.5	5.26	0.692	3.26E-08	1.52E-07	1.22E-02	3.28E-04	8.05E-08		
S6	3416	NA	NA	HCS6	spring	NA	DS	6.0	5.00	0.647	3.42E-08	1.57E-07	1.14E-02	2.98E-04	7.34E-08		
S7	3469	NA	NA	HCS7	spring	NA	DS	0.5	6.00	0.660	3.34E-08	1.52E-07	1.21E-02	3.28E-04	8.26E-08		
S8	3313	NA	NA	HCS8	spring	NA	DS	8.1	0.64	0.684	3.99E-08	1.78E-07	1.30E-02	3.21E-04	7.64E-08		
S9	3408	NA	NA	HCS9	spring	NA	DS	0.2	5.5	0.673	3.39E-08	1.58E-07	1.24E-02	3.34E-04	8.91E-08		
S10	3457	NA	NA	HCS10	spring	NA	DS	5.4	7.24	0.677	3.28E-08	1.48E-07	1.13E-02	3.01E-04	7.60E-08		
HCSW1	3416	0.9	4.0	HCSW1-5ft	S well	1.5	DS	3.2	0.19	0.935	6.28E-08	2.76E-07	2.01E-02	4.68E-04	NM		
HCBW1	3416	7.3	30.5	HCSW1-25ft	IB well	7.6	DS	3.2	0.5	1.240	1.19E-07	4.32E-07	2.67E-02	5.39E-04	NM		
				HCBW1-82ft	DB well	25.0	DS	3.3	0.05	1.282	1.53E-07	4.63E-07	2.76E-02	5.48E-04	NM		
HCSW2	3394	1.5	7.6	HCSW2-6ft	S well	1.8	DS	2.8	0.22	0.960	5.37E-08	2.25E-07	2.08E-02	4.77E-04	1.13E-07		
HCBW2	3394	11.7	40.4	HCBW2-38ft	IB well	11.6	DS	2.4	0.20	1.474	1.41E-07	5.78E-07	3.24E-02	6.28E-04	NM		
				HCBW2-121ft	DB well	36.9	B/CCT	NM	NM	NM	1.83E-07	5.05E-07	4.24E-02	7.34E-04	NM		
HCCW3	3378	0.0	3.0	HCCW3-5ft	S well	1.5	DS	1.2	9.7	0.660	3.43E-08	1.55E-07	1.22E-02	3.29E-04	8.00E-08		
HCFW3	3378	4.3	9.1	HCFW3-17ft	S well	5.2	DS	2.2	0.26	1.080	9.45E-08	3.65E-07	2.38E-02	5.18E-04	NM		
HCBW3	3378	16.2	52.5	HCBW3-47ft	IB well	14.9	DS	2.7	0.0	1.198	1.09E-07	4.02E-07	2.61E-02	5.42E-04	NM		
				HCBW3-157ft	DB well	47.9	B/CCT	NM	NM	NM	1.30E-07	3.42E-07	3.16E-02	5.96E-04	NM		
HCBW4	3361	16.8	45.7	HCBW4-Int	IB well	21.3	P/CCT	4.1	0.18	NM	7.81E-08	2.96E-07	1.98E-02	4.23E-04	NM		
				HCBW4-76ft	DB well	23.2	DS	2.3	5.25	1.194	9.91E-08	4.08E-07	2.53E-02	5.01E-04	1.05E-07		
				HCBW4-145ft	DB well	44.2	B/CCT	NM	NM	NM	9.84E-08	3.22E-07	2.77E-02	5.29E-04	NM		
HCFW5	3303	0.6	6.9	HCFW5-5ft	IB well	1.5	DS	3.0	0.0	1.080	9.23E-08	3.62E-07	2.33E-02	5.32E-04	NM		
WP2	3508	4.6	236.3	WP2-15m	DB well	14.9	B/CCT	5.6	4.5	NM	3.87E-08	1.73E-07	1.45E-02	3.60E-04	NM		
				WP2-100ft	DB well	30.5	B/CCT	10.1	6.04	NM	4.79E-08	2.07E-07	1.58E-02	3.67E-04	NM		
				WP2-60m	DB well	60.1	B/CCT	4.7	2.5	NM	4.63E-08	1.95E-07	1.63E-02	3.94E-04	NM		
				WP2-475ft	DB well	144.8	B/CCT	9.8	3.53	NM	4.40E-08	1.96E-07	1.38E-02	3.40E-04	NM		
				WP2-650ft	DB well	198.2	B/CCT	9.5	0.88	NM	4.66E-08	1.78E-07	1.44E-02	3.77E-04	NM		
				WP2-220m	DB well	220.1	B/CCT	4.9	0.5	NM	5.09E-08	2.02E-07	1.25E-02	3.16E-04	NM		
WP4	3571	open ^c	open ^c	WP4-55m	DB well	54.9	B/CCT	15.4	0.0	NM	2.97E-07	4.40E-07	3.07E-02	6.27E-04	NM		
				WP4-110m	DB well	110.1	B/CCT	12.0	0.5	NM	8.05E-07	7.44E-07	5.04E-02	8.38E-04	NM		

^a Abbreviations are T, temperature; DO, dissolved oxygen; TGP, total dissolved gas pressure; atm, atmospheres; cm³ STP/g, cubic centimeters per gram of water at standard temperature and pressure; S well, shallow well; IB well, integrated bedrock well; DB well, discrete bedrock well; NA, not applicable; DS, diffusion sampler; B/CCT, bailed clamped copper tube; P/CCT, pumped clamped copper tube; NM, not measured.

^b Read 3.32E-08 as 3.32 × 10⁻⁸.

^c Hole open to 123 m.

tributing flow. Aquifer test results indicate K values are in the 10^{-6} – 10^{-5} m/s range for the surficial deposits and in the 10^{-9} – 10^{-6} m/s range for the bedrock [Caine *et al.*, 2006]. Artesian conditions exist in the bedrock near the trunk stream. Measured static water levels in the bedrock HC wells are up to 3 m above ground surface. Sustained or seasonal artesian flow occurs in all of the bedrock HC wells (maximum of 1.3 L/s) except HCBW4, which is set back about 60 m from the stream. Water levels are generally 30–130 m below land surface and vary up to 50 m/yr in the upper part of the watershed. Close to the stream, water levels are near or above land surface and vary by <3 m/yr [Caine *et al.*, 2006]. Assuming the water table mimics topographic throughout the watershed, the dominant groundwater flow direction should be toward the trunk stream given that the topographic gradient is about 5 times greater perpendicular to the trunk stream than parallel to it.

4. Sample Collection and Analysis

[16] Temperature profiles were measured in 2003 and 2004 using a standard downhole temperature/conductivity logging tool manufactured by either Auslog, Mount Sopris, or Century, having a rated precision of $\leq 0.01^\circ\text{C}$. The tool was field-calibrated using two standards straddling the range of anticipated temperature measurements. Temperatures of the standards were determined using two handheld probes, each with rated accuracy of 0.1°C . Temperatures were recorded every 0.5–3.0 cm, depending on the tool. Logging rates were 1.5–3.0 m/min, and the tool was stopped for several minutes immediately after submersion at the water table to allow complete thermal equilibration.

[17] Thirty-two samples for dissolved gas and tritium were collected from 10 springs and 11 wells (Table 1) in late summer and fall of 2003. Dissolved gas samples were collected using multiple techniques (Table 1). Passive diffusion samplers similar to those described by Sanford *et al.* [1996] were used in combination with a total dissolved pressure probe [Manning *et al.*, 2003] for spring samples and well samples from depths <30 m. For springs, diffusion samplers were placed directly in the spring orifice to ensure that sampled waters had not reequilibrated with the atmosphere. An approximately 2.5-m-long Kemmerer sampling bottle was used to collect discrete samples from depths >30 m, along with one sample from a depth of 15 m in well WP2. Immediately after the bottle was hauled to the surface, it was drained through a valve in the bottom and a clamped copper tube sample was collected as described by Stute and Schlosser [2000]. A submersible pump was used to collect one sample (clamped copper tube) from well HCBW4 in an attempt to collect a flow-weighted sample (see below) because this well is not artesian. Tritium samples were collected either as grab samples (springs) or with the Kemmerer bottle (wells), except for the one pumped sample from well HCBW4.

[18] Samples can be divided into four types: (1) spring samples; (2) shallow well samples; (3) discrete bedrock well samples; and (4) integrated bedrock well samples (Table 1). Spring samples were collected from perennial (in 2003) springs located next to the stream (Figure 2). Spring and shallow well samples were collected to characterize groundwater in materials overlying the bedrock. Discrete bedrock well samples were collected from different depths in wells

WP2 and WP4 in an attempt to identify age profiles in the upper part of the watershed. Wells WP1 and WP3 were not sampled because they were obstructed above the water table in 2003. Well WP1 was reopened in 2004 but not sampled because of potential drilling water contamination. Discrete bedrock samples were also collected from near the bottom of bedrock HC wells (except HCFW5) in order to characterize groundwater at deeper levels of the bedrock aquifer near the stream.

[19] Integrated bedrock well samples were collected from the top of the screen in bedrock HC wells. The fact that four of five of these wells has artesian flow means that these samples should integrate a broad spectrum of flow paths in the bedrock en route to the stream, thereby approximating a flow-weighted sample. To evaluate this assumption, a simple two-dimensional (2-D) finite element model of the bedrock aquifer was constructed using FEFLOW [Diersch, 1998]. The 2-D vertical section is oriented perpendicular to the stream, $z = 100$ m, and $K = 5 \times 10^{-7}$ m/s (homogeneous and isotropic). Boundary conditions are constant head equal to the land surface at the stream, $R = 10$ cm/yr along the top of the model, and no-flow elsewhere. Steady state and transient model runs were performed with and without wells installed next to the stream with depths of 8, 28, and 52 m (similar to bedrock HC wells). This modeling exercise revealed the following. First, 2–3 weeks after well installation (when samples were collected), the 8-, 28-, and 52-m deep wells captured 83%, 93%, and 94% of the aquifer discharge, respectively, i.e., the considerable majority. Second, although the flow system requires about a year to reequilibrate to a new steady state, the relative flow distribution in the wells 2–3 weeks after installation is nearly identical to that at steady state. These results support the assumption that the integrated samples do indeed approximate flow-weighted samples. They also suggest that wells penetrating only the upper part of the bedrock aquifer integrate groundwater flow nearly as effectively as deeper wells. This modeling exercise does not take into account groundwater flow parallel to and underneath the stream. However, the volume of this underflow is presumably small in comparison with the volume of groundwater flowing toward and discharging into the stream, given the narrowness of the drainage bottom and the fact that the topographic gradient is considerably steeper perpendicular to the stream than parallel to it.

[20] The integrated sample from well HCBW4 was collected using a submersible pump and pumping at a relatively high flow rate because this well is not artesian. The integrated sample from HCBW4 is therefore probably biased toward the younger part of the age spectrum in the bedrock aquifer and is thus a poorer approximation of a flow-weighted sample than the other integrated samples. However, the fact that the well screen is long (29 m) and the well is still relatively close to the stream (60 m away) means that it should still roughly approximate a flow-weighted sample.

[21] Tritium analyses were performed at the USGS Noble Gas Laboratory in Denver, Colorado. Tritium analyses were performed using the ^3He in-growth method [Bayer *et al.*, 1989]. The detection limit is approximately 0.05 tritium units (TU). Analytical uncertainty ranges from 0.05 TU at low concentrations (≤ 1 TU) to 0.2 TU at higher concen-

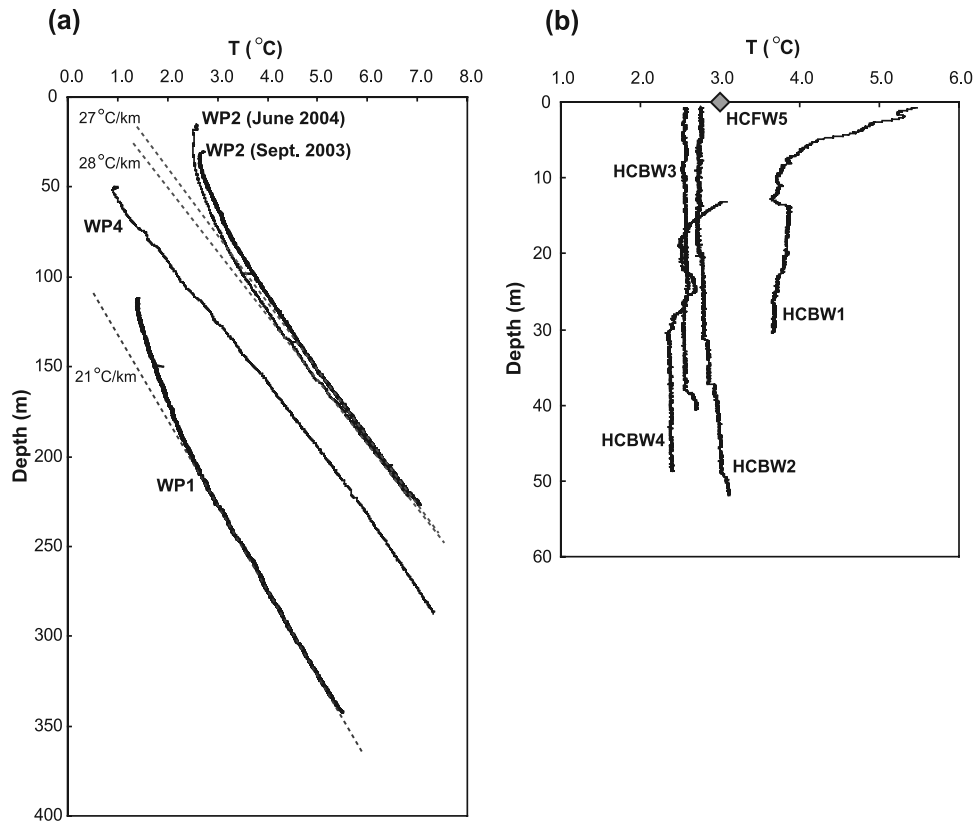


Figure 3. Temperature profiles from bedrock wells. All start at the water table. (a) WP wells. Dashed line is conductive geothermal gradient inferred from the lower linear portion of the profile. (b) Bedrock HC wells. Only a point measurement was collected at the surface from HCFW5 (flowing well) because it is only 7 m deep.

trations (≥ 5 TU). Dissolved gas samples collected in clamped copper tubes were analyzed at the USGS Noble Gas Laboratory for He, Ne, Ar, and N_2 concentrations and the $^3\text{He}/^4\text{He}$ ratio. Dissolved gases were extracted from samples on an ultrahigh vacuum extraction line. Nitrogen was measured on a quadrupole mass spectrometer in dynamic operation mode, and then reactive gases were removed using a Ti/Zr sponge. Noble gases were separated cryogenically and then measured using separate aliquots on a magnetic sector mass spectrometer run in static operation mode. Measurement uncertainties (1σ) are 1% for He, 3% for Ne, 2% for Ar, 2% for N_2 , and 1% for $^3\text{He}/^4\text{He}$ ratio. Dissolved gas samples collected in diffusion samplers were analyzed at the University of Utah Noble Gas Laboratory for He, Ne, Ar, Kr, and N_2 concentrations and the $^3\text{He}/^4\text{He}$ ratio using procedures described by Manning and Solomon [2004]. Krypton concentrations could not be determined for samples with high gas concentrations (Table 1). Measurement uncertainties (1σ) are 1% for He, 2% for Ne, 2% for Ar, 5% for Kr, 2% for N_2 , and 1% for $^3\text{He}/^4\text{He}$ ratio.

5. Results

5.1. Temperature Profiles

[22] Temperature profiles from WP1 and WP2 are relatively smooth and do not suggest the presence of large, discrete inflows and outflows (Figure 3a). Both profiles have an upper curved segment and a lower linear segment.

Curved segments are concave upward, indicative of downward flow (recharge) and/or lateral flow from higher elevations. Linear segments have slopes of $21^\circ\text{--}28^\circ\text{C}/\text{km}$, consistent with expected conductive geotherms for the Front Range ($20^\circ\text{--}25^\circ\text{C}/\text{km}$) [Birch, 1950; Decker, 1969]. In WP1, the profile becomes conductive at a depth of about 210 m, or about 100 m below the water table. Flowmeter results from WP1 under ambient conditions show no detectable flow. The detection limit of the heat pulse flow meter is 6×10^{-3} L/s, well above expected ambient downward flow rates in the formation, assuming recharge is of the order of 10 cm/yr. Therefore the absence of detectable flow using the flowmeter is expected; the presence of detectable flow suggests that the borehole is disturbing the flow field by focusing vertical flow. In WP2, the September 2003 and June 2004 profiles become conductive at about 140 and 160 m, respectively, or at depths of about 110 and 140 m, respectively, below the water table. The higher water table in June appears to drive flow slightly deeper. Flowmeter data collected in September 2003 indicate downflow to a depth of 127 m, suggesting that the borehole probably is enhancing downflow, and may locally increase the depth of the active zone. In summary, the WP1 and WP2 profiles are consistent with diffuse flow in the active zone associated with pervasive fractures and suggest a general maximum circulation depth of about 200 m, or about 150 m below the water table. A maximum active zone thickness of about 200 m is consistent with

estimates by *Robinson et al.* [1974] for a nearby area of the Front Range (80–160 m), and with most estimates (100–200 m) for bedrock aquifers in other mountainous areas [e.g., *Tiedeman et al.*, 1998; *Desbarats*, 2002; *Mayo et al.*, 2003].

[23] The profile from WP4 is also relatively smooth (Figure 3a). However, it is gently convex upward throughout, indicative of upward flow. This is unexpected, given its position high in the watershed. Flowmeter data indicate upflow from 80 to 120 m, the maximum depth that could be logged due to an obstruction. This upflowing water is older than any other sampled in the watershed (see section 5.3), including water at depth under the stream. We therefore suspect that WP4 penetrated a pressurized, permeable fracture or fracture network in the inactive zone, inducing the upward flow of water that was relatively stagnant prior to drilling. The WP4 profile therefore cannot be used for determining the depth of the active zone.

[24] Thermal profiles from HCBW1, HCBW2, and HCBW3 (Figure 3b) are overall very steep below the zone of seasonal temperature oscillation (depth >10 m), as expected for artesian wells. Warmer temperatures in the upper 10 m of HCBW1 are probably due to the lower artesian flow rates in this hole compared with HCBW2, HCBW3, and HCFW5 (allowing some near-surface thermal equilibration), and/or some contribution of warmer near-surface groundwater to the artesian flow (flowmeter data do indicate more upflow at shallower depths). The profile from HCBW4 is also overall very steep. Flow metering in HCBW4 indicates downflow to a depth of 29 m, and flow above the detection range (in an unknown direction) below 29 m where the thermal profile becomes essentially vertical. Only a point temperature measurement was made of water discharging from HCFW5 because of its shallow depth. The most noteworthy characteristic of these profiles is that temperatures in the bedrock aquifer from HC2 downstream to HC5 are very similar, only ranging from 2.4° to 3.1°C. Temperatures in the bedrock (depth >10 m) at HC1 are warmer, ranging from 3.7° to 3.9°C, suggesting longer residence times due to either a larger z , a smaller R , or a larger n in this part of the watershed.

5.2. Dissolved Gas Data

[25] Tables 1 and 2 show dissolved gas concentrations and derived recharge parameters. Recharge parameters were derived assuming the closed-system equilibration (CE) model [*Aeschbach-Hertig et al.*, 2000] in which noble gas concentrations are controlled by four parameters: recharge elevation (H_r); recharge temperature (T_r); entrapped air at the water table (A_e); and the fractionation factor (F). H_r and T_r are the elevation and temperature of the water table, respectively, at the point of recharge. A_e and F control excess air entrainment, excess air being the component of dissolved atmospheric gases in excess of solubility levels [*Heaton and Vogel*, 1981]. Excess air is ubiquitous in groundwater and is believed to result from the entrapment and subsequent dissolution of air bubbles during water table rises [*Kipfer et al.*, 2002]. A_e is the amount of air trapped when the water table rises, and F describes the degree to which the atmospheric gases become fractionated during dissolution. Solving for all four of these parameters simultaneously is not possible given current levels of analytical

precision because some of them are highly correlated [*Aeschbach-Hertig et al.*, 1999], so a value is typically assumed for H_r . In this study, H_r was assumed to be the approximate mean elevation of the portion of the watershed up-gradient from the sample location (assuming the water table mimics topography) and has an uncertainty of about ± 150 m.

[26] Values for T_r , A_e , and F were derived from measured concentrations of Ne, Ar, Kr, and N_2 using a chi-square minimization method similar to those described by *Aeschbach-Hertig et al.* [1999] and *Ballentine and Hall* [1999]. Unfortunately, Kr concentrations could not be measured for most samples due to high gas concentrations. Chi-square (χ^2) is a measure of the misfit between measured and modeled parameters, and its magnitude indicates the probability that the model indeed describes the data. The χ^2 distribution is only defined for cases where the number of measured gases exceeds the number of parameters; if the number of parameters and measured gases is the same, then χ^2 minimization can still be used to derive parameters, but the χ^2 value essentially provides no information on the acceptability of the fit (probability that the model describes the data). Therefore a value was assumed for T_r when Kr concentrations were not available. Temperatures in the bedrock aquifer under the stream where most of the high gas samples were collected are dominantly 2°–3°C (Figure 3b), and water table temperatures in the watershed in locations where recharge is occurring range from 1° to 3°C (WP1, WP2, and HCBW4 in Figure 3). Accounting for the possibility of rapid infiltration of snowmelt, the range of possible T_r values is therefore only 0°–3°C, leading us to assume $T_r = 1.5^\circ\text{C}$ when Kr was unavailable. The resulting uncertainty in T_r of $\pm 1.5^\circ\text{C}$ is similar to that of derived T_r values when an adequate number of gases can be measured.

[27] Dissolved oxygen (DO) concentrations are commonly low (Table 1), raising the possibility that N_2 concentrations have been affected by denitrification. This possibility was evaluated for samples with DO levels <1 mg/L by deriving recharge parameters both with and without N_2 . Resulting differences in derived parameters were nontrivial for five samples (Table 2), four of these being the deepest discrete sample from the respective well. These four samples all had an apparent N_2 excess, and N_2 was excluded in the derivation of recharge parameters. Spring samples HCS2 and HCS4 were apparently stripped, having low Ne and He concentrations resulting in unacceptably high χ^2 values (probability < 5%). Ne was not included in the derivation of recharge parameters for these samples, and its exclusion resulted in an acceptable χ^2 value. He was included in the derivation of recharge parameters for samples HCS6, WP2–15m, and WP2–475ft because excluding it resulted in a modeled He concentration >2% above the measured concentration, which is unlikely.

[28] Only five of 32 samples have unacceptably high χ^2 values (probability < 5%), and three of these are from WP2 and are potentially problematic for other reasons explained in section 5.3. Derived T_r values range from 0.0° to 7.1°C, with most being in the expected range of 0.0°–3.0°C. The three warmer T_r values (4.4°–7.1°C) are all from springs and probably reflect the influence of water with a residence time of weeks to months. Excess air (EA) in Table 2 is the

Table 2. Modeled Recharge Parameters and Ages^a

Sample Name	Assumed H ₂ O, m asl	T _b , °C	ΔNe, % solubility	EA, cm ³ STP/g	CE Model					UA Model χ ²	⁴ He _{em} , cm ³ STP/g	R/R _a	³ He*, TU	Apparent Age, years	Exponential Mean Age, years	Initial ³ H, TU	Notes ^b	
					A _e , cm ³ STP/g	F	v	q	χ ²									
HCS1	3537	0.8	1.7	0.0003	0.0532	1.0	1.0	1.02	0.02	0.05	1.43E-10 ^c	1.014	0.7	9.79	1.24	NC	10.5	
HCS2	3506	1.5	-7.1	0.0000	0.0000	1.0	1.0	1.00	0.71	0.71	1.59E-09	1.005	1.3	8.95	1.2	NC	8.6	1,2
HCS3	3476	7.1	11.5	0.0017	0.0874	0.9	1.0	1.10	0.02	0.09	5.94E-10	1.137	3.4	10.66	4.9	NC	14.1	
HCS4	3537	1.5	4.6	0.0049	0.1335	0.8	1.0	1.27	0.00	22.01	-3.79E-10	1.354	6.8	10.41	9.0	NC	13.0	1,2
HCS5	3567	0.4	2.1	0.0004	0.0531	1.0	1.0	1.02	0.33	0.47	-6.29E-10	1.035	0.7	8.02	1.4	NC	8.7	
HCS6	3567	4.5	10.4	0.0009	0.0156	0.9	0.9	1.06	2.01	2.79	-1.61E-10	0.993	0.1	7.86	0.3	NC	8.0	3
HCS7	3598	0.0	2.0	0.0002	0.0002	0.0	0.0	U	0.22	0.22	1.54E-10	0.997	0.4	9.70	0.7	NC	10.1	
HCS8	3476	4.4	23.6	0.0026	0.0132	0.7	0.8	1.16	0.24	0.98	-7.16E-10	1.027	0.6	10.70	0.9	NC	11.3	
HCS9	3598	0.9	7.1	0.0012	0.5000	0.9	1.0	1.06	1.38	2.66	-3.97E-10	1.000	0.1	12.55	0.2	NC	12.7	
HCS10	3598	3.0	3.2	0.0002	0.0002	0.0	0.0	U	0.14	0.14	-3.32E-10	0.994	0.1	9.61	0.1	NC	9.7	
HCSW1-5ft	3567	1.5	87.9	0.0120	0.0544	0.5	0.8	1.69	0.01	109.05	5.33E-10	1.419	15.3	12.17	14.5	NC	27.4	1
HCBW1-25ft	3567	1.5	193.8	0.0205	0.0357	0.2	0.4	2.20	0.42	56.78	1.58E-08	1.291	28.3	6.87	29.0	NC	35.1	1
HCBW1-82ft	3567	1.5	215.5	0.0217	0.0337	0.2	0.4	2.28	0.94	42.16	4.00E-08	1.127	32.9	5.06	35.9	NC	38.0	1
HCSW2-6ft	3537	1.5	52.7	0.0096	0.5000	0.6	1.0	1.52	0.70	183.13	3.75E-09	1.277	10.7	12.32	11.1	NC	23.0	1,4
HCBW2-38ft	3537	1.5	292.3	0.0287	0.0412	0.1	0.3	2.69	4.17	46.26	-9.67E-10	1.223	17.2	11.28	16.5	NC	28.5	1,5
HCBW2-121ft	3537	1.5	242.5	0.0327	0.1001	0.2	0.7	2.87	0.00	204.12	6.73E-08	1.156	52.7	11.09	31.1	NC	63.8	1,4
HCCW3-5ft	3537	1.5	4.8	0.0009	0.1594	1.0	1.0	1.05	0.25	0.49	3.73E-10	1.048	1.5	9.59	2.5	NC	11.1	
HCFW3-17ft	3537	1.5	147.5	0.0171	0.0404	0.3	0.6	1.99	1.29	83.52	1.01E-08	1.311	22.2	11.41	19.2	NC	33.6	1
HCBW3-47ft	3537	1.5	172.8	0.0198	0.0421	0.2	0.5	2.15	0.15	87.67	1.47E-08	1.361	30.3	11.51	22.9	NC	41.8	1
HCBW3-157ft	3537	1.5	132.1	0.0200	0.1184	0.4	0.8	2.12	0.00	195.88	5.38E-08	1.351	54.9	14.40	27.9	NC	69.3	1,4
HCBW4-Int	3537	1.5	101.1	0.0106	0.0196	0.3	0.5	1.62	0.43	16.72	7.03E-09	1.241	14.5	11.33	14.6	NC	25.8	1
HCBW4-76ft	3537	1.0	175.0	0.0177	0.0273	0.2	0.4	2.03	0.10	23.64	-4.18E-10	1.024	1.5	9.12	2.7	NC	10.6	
HCBW4-145ft	3537	1.5	118.4	0.0164	0.0690	0.4	0.8	1.93	0.00	116.35	2.55E-08	1.043	16.5	8.65	19.0	NC	25.2	1,4
HCFW5-5ft	3476	1.5	143.7	0.0171	0.0452	0.3	0.6	1.98	5.71	96.74	1.02E-08	1.451	29.0	15.56	18.7	NC	44.6	1,5
WP2-15m	3598	1.5	18.5	0.0035	0.1603	0.8	1.0	1.19	6.39	36.92	-1.76E-11	1.014	0.5	4.23	1.8	NC	4.7	1,3,5
WP2-100ft	3598	1.5	41.2	0.0053	0.0212	0.6	0.8	1.31	3.11	21.25	-9.03E-11	0.998	0.1	7.92	0.2	NC	8.0	1
WP2-60m	3598	1.5	33.6	0.0061	0.0815	0.7	0.9	1.34	5.88	71.72	1.12E-09	0.990	0.6	5.35	1.8	NC	5.9	1,5
WP2-475ft	3598	1.5	33.9	0.0030	0.0072	0.5	0.6	1.18	0.53	5.63	-6.45E-11	0.997	0.1	6.71	0.4	NC	6.9	1,3
WP2-650ft	3598	1.5	21.8	0.0042	0.2833	0.8	1.0	1.23	0.77	46.47	6.71E-09	0.973	3.2	7.44	6.4	NC	10.6	1
WP2-220m	3598	1.5	38.1	0.0019	0.0019	0.0	0.0	U	20.72	20.72	8.64E-09	0.981	4.3	7.81	7.9	NC	12.2	1,5
WP4-55m	3659	1.5	203.1	0.0262	0.0698	0.2	0.6	2.53	0.85	155.30	1.94E-07	0.258	-15.4	0.97	>50	NC	-14.4	1
WP4-110m	3659	1.5	412.4	0.0465	0.0832	0.1	0.4	3.74	0.00	118.82	6.26E-07	0.228	-4.1	1.25	>50	NC	-2.9	1,4

^aAbbreviations are H₂O, recharge elevation; T_b, recharge temperature; EA, excess air defined as the sum of the excess components of all atmospheric gases (except He); cm³ STP/g, cubic centimeters per gram of water at standard temperature and pressure; see text for definition of excess air parameters (A_e, F, v, q); χ², model misfit; ⁴He_{em}, terrigenous ⁴He; R/R_a, sample ³He/⁴He ratio divided by the atmospheric ³He/⁴He ratio; ³He*, tritiogenic ³He; TU, tritium unit; U, undefined; NC, not computed.

^bNotes are 1, T_b assumed; 2, Ne excluded in inversion because stripped, and excess air He component computed using Ne only; 3, He included in inversion because modeled concentration >2% above measured concentration if excluded; 4, N₂ excluded in inversion because apparent denitrification; 5, χ² unacceptably high.

^cRead 1.43E-10 as 1.43 × 10⁻¹⁰.

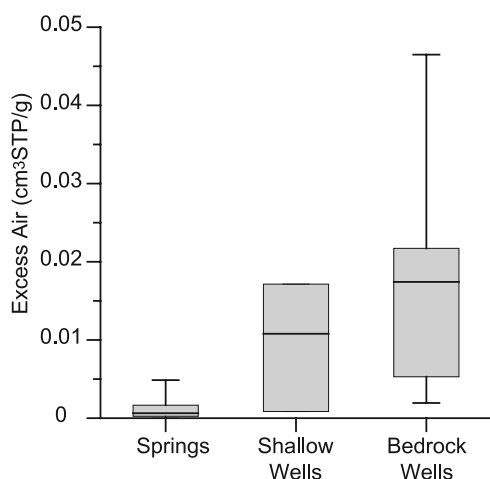


Figure 4. Box-whisker plot comparing excess air concentrations in spring samples, shallow well samples, and bedrock well samples. Excess air is the sum of the modeled excess atmospheric gas components.

sum of all modeled excess atmospheric gas components (including O_2). Note that the EA composition is approximately that of air, but not exactly because the CE model was used instead of the unfractionated excess air (UA) model [Kipfer *et al.*, 2002]. The Ne excess above solubility, expressed as ΔNe , traditionally has been used as a measure of excess air when the excess air is fractionated (as with the CE model) [Stute and Schlosser, 2000], so ΔNe is also presented for reference in Table 2. However, we believe that EA is a more complete expression of excess air, and will use it henceforth. Excess air concentrations range from 0 to $0.0465 \text{ cm}^3 \text{ STP/g}$, and consistently exceed $0.02 \text{ cm}^3 \text{ STP/g}$ ($\Delta Ne > 170\%$) in the bedrock HC wells and WP4. These EA concentrations are unusually high; typical concentrations are $<0.01 \text{ cm}^3 \text{ STP/g}$ ($\Delta Ne < 100\%$) [Wilson and McNeill, 1997; Stute and Schlosser, 2000]. The fact that many of the samples were collected with diffusion samplers rules out the possibility that the high EA concentrations are merely the result of bubbles stuck in sampling tubes. In general, EA levels are lowest in the spring samples, higher in the shallow well samples, and highest in the bedrock well samples, suggesting a general trend of increasing EA with depth (Figure 4), but this could be due in part to poorer gas confinement in the shallower samples (see section 6).

[29] Derived A_e values for bedrock samples are mainly $0.02\text{--}0.1 \text{ cm}^3 \text{ STP/g}$, similar to other reported values [Aeschbach-Hertig *et al.*, 2000]. Unusually high EA values for the bedrock samples are due to unusually low F values. The F parameter in the CE model is defined as $F = v/q$, where v is the fraction of the initial trapped gas volume at the water table remaining after excess air entrainment (after equilibrium conditions are reestablished), and q is the ratio of the dry gas pressure in the trapped gas to that in the local atmosphere. The q parameter therefore indicates the magnitude of the water table rise responsible for the EA. The low F values are due primarily to unusually high q values that range mainly from 1.9 to 3.7, compared with 1.1–1.6 for normal q values [Aeschbach-Hertig *et al.*, 2000]. This range of modeled q values indicates water table fluctuations of 3–15 m, which are large but well

within the range of observed water table fluctuations in the upper part of the watershed. The unusually large EA values observed in the bedrock aquifer are therefore consistent with the unusually large water table fluctuations observed in Handcart Gulch.

[30] The large bedrock EA concentrations make this data set an especially robust test of the CE model. Differences between gas concentrations calculated using the UA and CE models generally become larger with increasing EA concentrations, increasing the magnitude of misfit values resulting from application of an inappropriate model. For bedrock samples, χ^2 values for the UA model are commonly >40 (essentially 0% probability), whereas χ^2 values for the CE model are generally acceptable (Table 2). The partial reequilibration (PR) model [Stute *et al.*, 1995; Aeschbach-Hertig *et al.*, 2000] was also applied to bedrock well samples for comparison. Resulting χ^2 values were generally acceptable as with the CE model. Derived A_d values (the amount of excess air initially dissolved) were mainly $0.05\text{--}0.10 \text{ cm}^3 \text{ STP/g}$, indicating water table fluctuations of 50–100 m. This range exceeds observed water table fluctuations in the watershed but cannot be ruled out. Yet the PR model demands that 70–90% of the Ne initially dissolved subsequently escaped by diffusion across the water table for most of the bedrock samples. A simple calculation was performed using Fick's law to evaluate the plausibility of this scenario. Assumptions included (1) a diffusion distance of 10 m, a minimum based on A_d values and observed water table fluctuations; (2) a constant Ne concentration at the water table equal to solubility; and (3) a constant Ne concentration at 10 m below the water table equal to the initial concentration indicated by A_d (an impossibility, but this results in maximum diffusion velocity). Under these conditions, about 100 years would be required to lose about 70% of the initial excess air Ne by diffusion, which is clearly problematic given downward average linear flow velocities $\geq 10 \text{ m/yr}$.

[31] In contrast to the rest of the bedrock samples, EA values for WP2 samples are not unusually high. This is unexpected given that the largest water table fluctuations were observed in WP2. The well was drilled using stream water (probably with low EA) 2 years prior to sampling. It is probable that the well is still contaminated, particularly at depths $>160 \text{ m}$ where thermal profiles indicate very low flow rates (also see age results in section 5.3). However, this seems unlikely at shallower depths where thermal profiles and flowmeter data indicate active flow, particularly at $<50 \text{ m}$ in the zone of annual water table fluctuation. Resampling the well in the future might help explain the apparent conflict.

5.3. $^3\text{H}/^3\text{He}$ Ages

[32] Apparent $^3\text{H}/^3\text{He}$ ages [Schlosser *et al.*, 1988, 1989] range from 0.1 to 35.9 years (Table 2) and generally have an uncertainty of 0.5–2.0 years. Initial ^3H values (measured $^3\text{H} +$ measured tritiogenic ^3He) were compared with the precipitation ^3H record (input curve) to evaluate the possibility that the samples contain a significant fraction of water recharge prior to 1950 (prebomb water) (Figure 5a). On a plot of initial ^3H versus apparent $^3\text{H}/^3\text{He}$ recharge year, samples should plot close to the input curve; samples plotting significantly below it probably have a significant

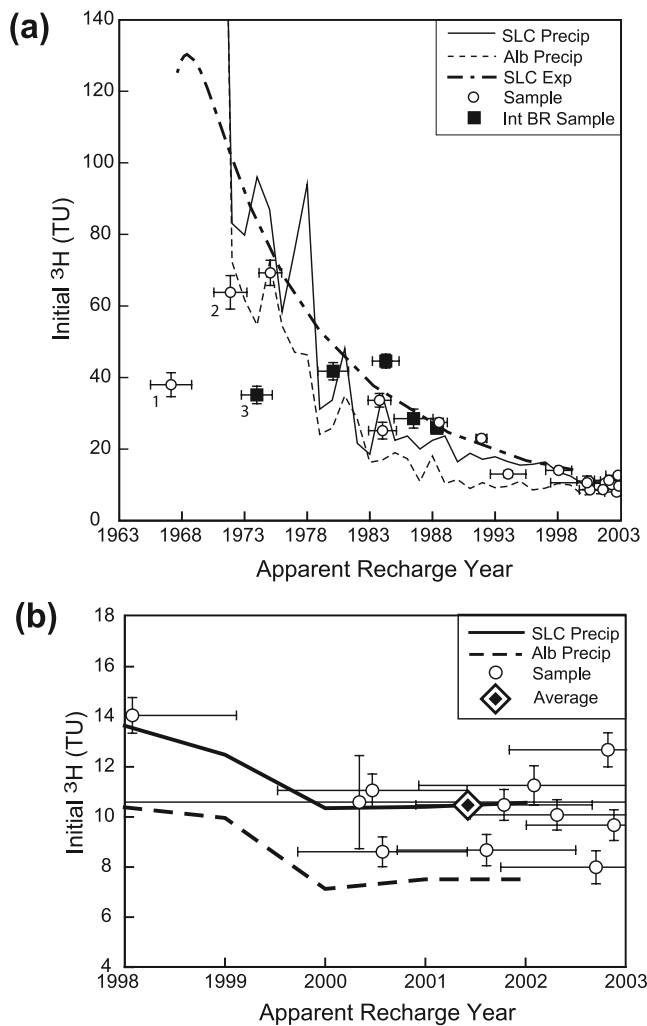


Figure 5. Apparent recharge year (from apparent $^3\text{H}/^3\text{He}$ age) versus sample initial ^3H concentration (measured $^3\text{H} +$ tritiogenic ^3He). Precipitation ^3H records for Salt Lake City, Utah (SLC precip) and Albuquerque, New Mexico (Alb precip), constructed from mean annual average concentrations, are shown for comparison. (a) All samples. A curve representing expected initial ^3H concentrations for samples with an exponential age distribution (SLC exp), calculated from the Salt Lake City record, is also shown for comparison with integrated bedrock well samples (int BR sample). Labeled samples are 1, HCBW1–82ft; 2, HCBW2–121ft; 3, HCBW1–25ft. (b) Samples with apparent ages <5 years. A point representing the average of these samples is also shown.

component of prebomb water [Stute *et al.*, 1997; Aeschbach-Hertig *et al.*, 1998; Manning *et al.*, 2005]. For samples plotting below the input curve, the apparent $^3\text{H}/^3\text{He}$ age is only representative of the fraction of the sample recharged after 1950 (modern fraction). The three closest available precipitation ^3H records were from Denver, Colorado, Salt Lake City, Utah, and Albuquerque, New Mexico [International Atomic Energy Agency, 2006]. The Denver record was too short (1963–1968) to allow construction of a reliable complete record by correlation. Complete records were constructed for Salt Lake City and Albuquerque by correla-

tion with Ottawa and Vienna records as described by Manning *et al.* [2005] (Figure 5a).

[33] Although both records are shown on Figure 5a for comparison, we believe precipitation ^3H at the site more closely matches the Salt Lake City record than the Albuquerque because (1) initial ^3H values for samples with apparent ages <5 years (least likely to contain prebomb water) plot closer to the Salt Lake City record (Figure 5b); and (2) for those years in which Denver precipitation concentrations are available, they are closer to Salt Lake City concentrations. The Salt Lake City record was therefore used to evaluate the presence of prebomb water and to compute exponential ages and will be henceforth referred to as the input curve for the site. Most samples plot relatively close to the input curve (Figure 5a), indicating that they contain little prebomb water. The exceptions are the three samples with the oldest apparent ages, HCBW1–82ft, HCBW1–25ft, and HCBW2–121ft. Of these, HCBW1–82ft probably contains the most prebomb water (and thus has the oldest residence time), followed by HCBW1–25ft and then HCBW2–121ft. Samples from WP2 are excluded from Figure 5 and from all following figures in which apparent age is plotted because of previously mentioned concerns about drilling water contamination. Notably absent in Figure 5 are mixtures of very old and very young water that might be expected in a highly heterogeneous flow system.

[34] Mean groundwater ages for the integrated bedrock well samples were computed from their apparent ages using the ^3H input curve assuming that these samples contain an exponential age distribution [Vogel, 1967; Cook and Böhlke, 2000] (Table 2). A curve indicating expected initial ^3H values for samples with exponential age distributions was also computed (Figure 5a). This curve is close to a smoothed version of the input curve but is slightly above it for recharge years in the 1980s. Initial ^3H values for four of the five integrated samples, all with recharge years in the 1980s, also plot slightly above the input curve, relatively close to the exponential curve. HCBW1–25ft is the exception, plotting well below the exponential curve. ^3H and ^3He concentrations in four of the five integrated samples are therefore consistent with exponential age distributions.

[35] Apparent ages from springs and HC wells are plotted relative to distance down the stream in Figure 6. Spring sample ages are the youngest (mainly <3 years), followed by shallow well samples (11–19 years) and then bedrock well samples (mainly 15–36 years). Discrete bedrock samples collected from near the bottom of the bedrock HC wells have the oldest apparent ages in each location. The apparent ages along with initial ^3H (Figure 5a) and terrigenic He concentrations (Table 2) all indicate that groundwater ages in the vicinity of the stream increase with depth. Terrigenic He (He_{terr}) is the component of He, other than tritiogenic He, with a nonatmospheric source, most likely some combination of U-Th series decay in crustal rocks and diffusion from the mantle. Because of its subsurface source, He_{terr} typically increases with age [Solomon, 2000]. Exponential mean ages for the integrated samples are also shown. Exponential mean ages from HC2 to HC5 are remarkably uniform, ranging from 8 to 11 years. The ^3H and He data are therefore generally consistent with a uniform flow system downstream of HC2, which includes most of the site. Note that

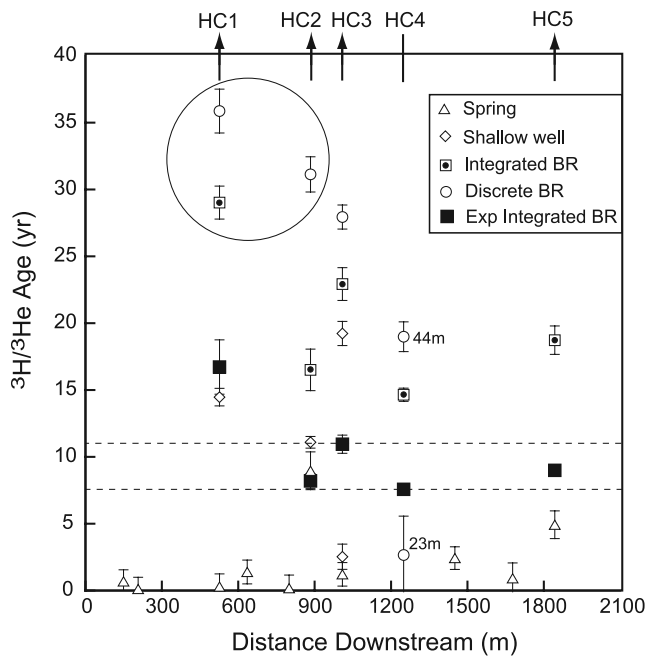


Figure 6. Distance downstream versus apparent $^3\text{H}/^3\text{He}$ age for springs and HC well samples. BR means bedrock. Exponential mean ages for the integrated bedrock well samples (exp integrated BR) are also shown. Sample depths are shown next to the two discrete bedrock samples from HCBW4. Encircled wells have significant prebomb fractions. Dashed lines indicate zone of variation of exponential ages for integrated bedrock samples, HCBW1–25ft excepted. Arrows at top indicate artesian flow in bedrock well.

ages for the integrated samples do not increase with distance downstream, as might be expected if stream-parallel groundwater flow were a significant component of the flow system. Apparent ages, the exponential mean age, and initial ^3H concentrations from HC1 all indicate that bedrock groundwater at this location is older than at other HC locations, consistent with anomalously warm bedrock groundwater temperatures (Figure 3b).

[36] ^3H concentrations in the two WP4 samples are 1.3 and 1.0 TU, the lowest measured at the site (Table 2), and indicative of predominantly prebomb water. He_{terr} concentrations in WP4 samples are in the $10^{-7} \text{ cm}^3 \text{ STP/g}$ range, at least an order of magnitude higher than the other samples, and possibly indicative of water hundreds to thousands of years old [Solomon, 2000]. The ^3H and He data therefore indicate that water in WP4 is the oldest sampled, despite the well's location relatively high in the watershed. This in combination with observed upflow in WP4 suggests that the sampled water is from the inactive zone, entering the borehole below the sampled interval ($>110 \text{ m}$). Apparent ages of discrete samples from the active zone ($<150 \text{ m}$) in WP2 are all <2 years, showing no increase in age with depth. Inactive zone samples ($>150 \text{ m}$) are older (6–8 years) but far younger than expected given the scale of inactive zone vertical flow velocities (cm/yr) implied by the temperature profiles (section 2). We therefore suspect that WP2 is contaminated with local stream water used during drilling

1 year prior to sampling. Apparent ages for the two samples collected within the zone of seasonal water table fluctuation ($<50 \text{ m}$) are arguably representative of aquifer waters, but deeper samples are considered unreliable.

6. Discussion

[37] Because both EA and apparent age increase with depth (Figures 4 and 6), EA should be correlated with apparent age, and Figure 7 shows that this is indeed the case. As expected, q values are similarly correlated with apparent age, suggesting that older samples were recharged in locations with larger water table fluctuations. We propose a simple explanation of this relationship, consistent with a uniform flow system, in which older waters are recharged farther from the creek at higher elevations, where seasonal water table fluctuations are larger (Figure 8). The fact that EA levels are similarly elevated in all the bedrock HC wells ($0.015\text{--}0.03 \text{ cm}^3 \text{ STP/g}$) suggests that water table fluctuations are similarly large at high elevations throughout the watershed (not just where wells are located), also consistent with a uniform flow system.

[38] One concern regarding EA-depth and age-depth correlations is potential sampling bias created by poorer gas retention for shallow samples. For the purpose of this discussion, the “sampling pressure” is considered to be the pressure (above atmospheric pressure) maintained on the sample during sample collection expressed in terms of the height of a water column required to exert that

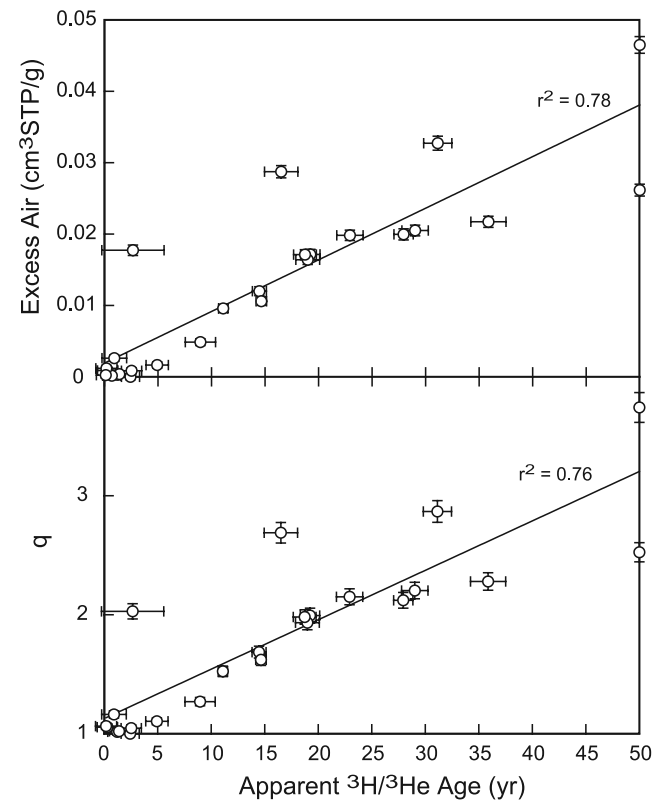


Figure 7. Apparent $^3\text{H}/^3\text{He}$ age versus excess air and q . Excess air is the sum of the modeled excess atmospheric gas components. Samples from WP4 with an apparent age >50 years are plotted with an age equal to 50 years.

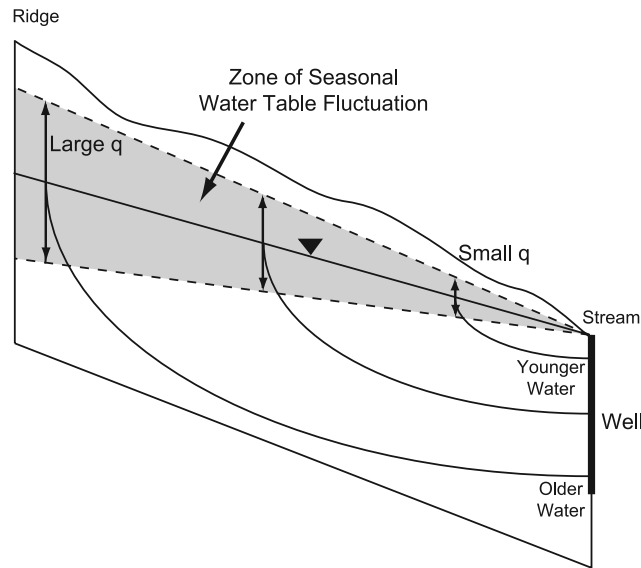


Figure 8. Cross section showing proposed explanation for correlation between q and apparent $^3\text{H}/^3\text{He}$ age.

pressure. Downhole total dissolved gas pressure probe readings from bedrock HC wells (Table 1) indicate that sampling pressures of at least 5 m are generally required to assure full gas retention for bedrock groundwaters. Therefore several samples may have lost gas, including spring samples (sampling pressure essentially = 0 m), bailed samples (sampling pressure = 1–2 m), and samples collected with diffusion samplers at depths <5 m (Table 1). The first scenario of concern is that all samples originally had high EA levels, but samples collected at progressively shallower depths (lower sampling pressures) lost progressively more gas, leading to an apparent EA-depth correlation. This scenario cannot be ruled out for the spring samples; they have both the lowest sampling pressures and the lowest average EA (Figure 9). Bubbles were observed in the spring pool during collection of sample HCS4, the spring with the highest modeled EA, indicating that gas was indeed probably lost from this sample. However, well samples with low sampling pressures, including bailed samples and diffusion samplers collected at depths <2 m, are not consistent with this scenario. If EA values were mainly controlled by sampling pressure, then these samples should all have similar EA values that fall mainly between those of spring samples and those of well samples having high sampling pressures (>5 m). Instead, they have EA values that span nearly the entire range for the site (Figure 9). It therefore appears that although spring samples are probably incapable of preserving high EA levels like those in the bedrock aquifer, sample pressures >1 m are (at least partially), and the EA-depth correlation cannot be completely explained by sampling bias.

[39] The second scenario of concern is that all samples originally had apparent ages similar to the bedrock well samples (>15 years), and samples collected at shallower depths have younger ages only due to gas loss. Gas loss will decrease apparent ages through the loss of tritogenic ^3He and by decreasing measured $^3\text{He}/^4\text{He}$ ratios as a result of fractionation between exsolved bubbles and the remaining

fluid. Potential changes in apparent ages due to gas loss were computed for the integrated bedrock samples assuming loss of the entire excess air component of He (worst-case scenario). Apparent ages do drop significantly to the 5- to 10-year range but still remain above the apparent ages of most spring samples (<2 years) because their consistently higher $^3\text{He}/^4\text{He}$ ratios (R/R_a in Table 2) are largely preserved. Therefore the age-depth correlation can be only partly explained by degassing.

[40] If varying degrees of gas loss were the main cause of observed variations in EA and age, and thus the EA-age correlation, then samples with similar sampling pressures should exhibit little or no correlation between EA and apparent age. Figure 10 demonstrates that this is not the case for spring samples and well samples with low sampling pressures, both sample types exhibiting a clear EA-age correlation. A final argument against significant gas loss is the fact that gas concentrations generally fit the CE model well. If degassing had occurred, one would expect a fractionation pattern that could not be described by the CE model.

[41] The most distinctive characteristics of dissolved gases in the Handcart Gulch bedrock aquifer are the unusually high EA concentrations and the correlation between EA and age. An important question is whether or not these characteristics are typical of alpine bedrock aquifers. Other dissolved gas data collected in the mountains exhibit normal EA concentrations of <0.01 cm^3 STP/g [Manning *et al.*, 2003; Rademacher *et al.*, 2001; Holocher *et al.*, 2001; Plummer *et al.*, 2001; Rauber *et al.*, 1991; Zuber *et al.*, 1995; Mazor *et al.*, 1983], with only a few exceptional samples [Rademacher *et al.*, 2001; Mazor *et al.*,

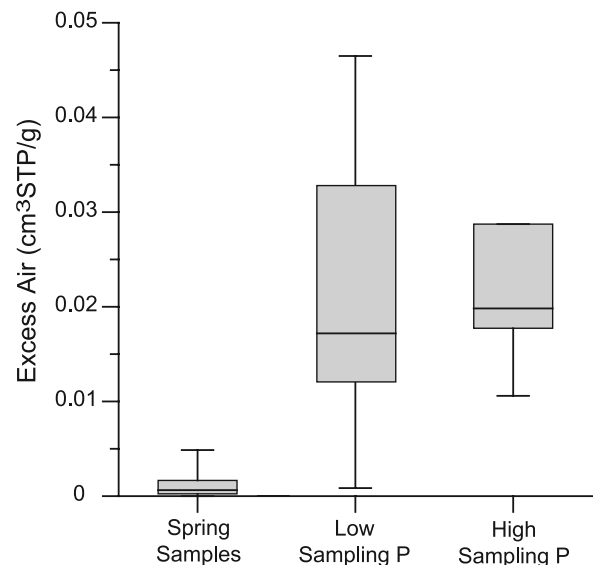


Figure 9. Box-whisker plot comparing excess air concentrations in spring samples, samples with low sampling pressure (<5 m), and samples with high sampling pressure (>5 m). Sampling pressure is the pressure (above atmospheric pressure) maintained on the sample during sample collection expressed in terms of the height of a water column required to exert that pressure. P means pressure. Excess air is the sum of the modeled excess atmospheric gas components.

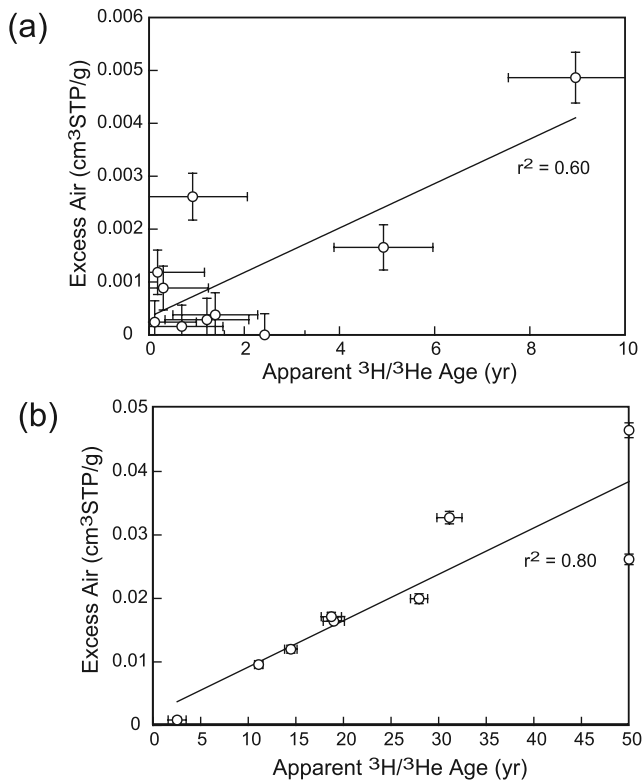


Figure 10. Apparent $^3\text{H}/^3\text{He}$ age versus excess air for (a) spring samples and (b) samples with low sampling pressures (<5 m). Excess air is the sum of the modeled excess atmospheric gas components. Samples from WP4 with an apparent age >50 years are plotted with an age equal to 50 years.

1983]. However, these data have generally been collected from (1) springs, which probably cannot preserve high EA concentrations; (2) shallow alluvial wells, which may not intercept bedrock waters; or (3) environments that are mountainous but not alpine. Dissolved gas data presented by *Johnson et al.* [2007] are an important exception. These data were collected from Prospect Gulch, an alpine watershed in the San Juan Mountains of Colorado at elevations >3100 m asl. Samples were collected from springs and wells completed at different depths, including a bedrock well located near the trunk stream at the bottom of the watershed. As in Handcart Gulch, the bedrock well is artesian, and samples from different depths in the well (27–41 m) have unusually high EA ($\Delta\text{Ne} > 200\%$). Bedrock wells higher in the watershed also show large water table fluctuations similar to those observed at Handcart Gulch. We therefore suspect that the high EA levels found in Handcart Gulch may be typical for alpine bedrock aquifers, and the primary reason they have not been found elsewhere is a lack of bedrock wells in alpine watersheds.

[42] A correlation between apparent tracer age and EA has been observed in other mountain settings [*Plummer et al.*, 2001; *Manning et al.*, 2003, Figure 4b]. Figure 11 shows modeled EA (expressed as ΔNe) plotted versus apparent $^3\text{H}/^3\text{He}$ ages for the previously described alpine groundwater samples presented by *Johnson et al.* [2007]. Samples with low sampling pressures (<1 m) and samples

with higher sampling pressures (>2 m) are plotted separately because gas loss is a concern, as at Handcart Gulch. EA and apparent age are clearly correlated, and the fact they are correlated for both sample types demonstrates that the correlation is not due to gas loss alone. Therefore we suspect that higher EA concentrations are commonly associated with older waters in alpine watersheds.

[43] In Handcart Gulch, the exponential mean ages for the integrated samples and the apparent ages of the spring samples imply a mean residence time of 8–11 years for most of the bedrock groundwater and <2 years for most of the shallow groundwater system feeding the springs. These mean residence times are similar to those calculated for deep/bedrock groundwater (5–9 years) and shallow groundwater (1–3 years) in other mountain watersheds using lumped parameter modeling [*Uhlenbrook et al.*, 2002; *Maloszewski et al.*, 1983; *Soulsby et al.*, 2000]. It should be understood that all mean residence times for fractured bedrock aquifers calculated from environmental tracer data may be older than the true mean residence time of the water due to diffusive exchange of the tracer between mobile fracture water and more immobile matrix water [e.g., *Cook et al.*, 2005]. For the purposes of this paper, however, relative age, not absolute age, is of primary importance.

7. Conclusions

[44] 1. Temperature profiles indicate active groundwater circulation to a maximum depth (aquifer thickness) of about 200 m, or about 150 m below the water table. Borehole temperature logging is a reliable method of identifying aquifer thickness in alpine watersheds underlain by fractured crystalline rock because linear profiles with slopes similar to the conductive geothermal gradient are reliable

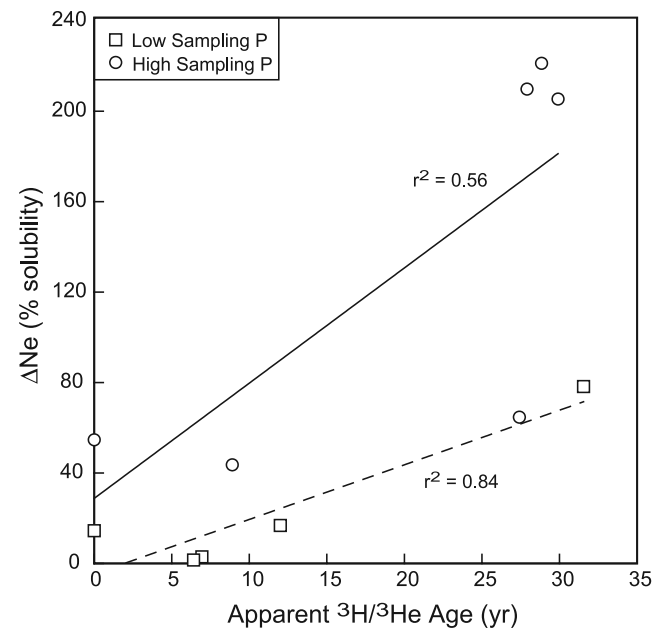


Figure 11. Apparent $^3\text{H}/^3\text{He}$ age versus excess air expressed as ΔNe for samples from Prospect Gulch, Colorado, from *Johnson et al.* [2007]. Separate linear regression lines are shown for samples with sampling pressures <1 m (dashed line) and >1 m (solid line).

indicators of very low flow velocities characteristic of the underlying inactive zone.

[45] 2. Dissolved noble gas data show unusually high excess air concentrations ($>0.02 \text{ cm}^3 \text{ STP/g}$, $\Delta\text{Ne} > 170\%$) in the bedrock, consistent with unusually large seasonal water table fluctuations (up to 50 m) observed in the upper part of the watershed. Dissolved gases are fractionated and support the CE model of excess air formation.

[46] 3. Apparent $^3\text{H}/^3\text{He}$ ages are positively correlated with sample depth and excess air concentrations. Although spring samples have probably experienced gas loss, the correlation cannot be attributed mainly to sampling bias. Most of the EA-age correlation is probably due to water table fluctuations increasing with distance from the stream.

[47] 4. Exponential mean ages for integrated bedrock well samples, assumed to be approximately flow weighted due to artesian flow, are remarkably consistent along the stream, four of five being from 8 to 11 years. This result in combination with other hydrologic and geologic data supports a simple watershed-scale conceptual model of groundwater flow in which permeability is primarily a function of depth and where recharge, aquifer thickness, and porosity are relatively uniform throughout most of the watershed. This result is surprising given the complexity of the bedrock geology. A flow system of this sort could be reasonably well represented with an equivalent porous media model calibrated with limited data, and such a model may yield useful information about solute transport and chemical mass balance within the watershed.

[48] **Acknowledgments.** This work was funded by the U.S. Geological Survey's Mendenhall Post-doctoral Research Fellowship Program, Mineral Resources Program within the Geologic Discipline, and Toxics Program within the Water Resources Discipline. We thank Charles Robinson of Mineral Systems, Inc., for graciously donating the deep boreholes to the USGS. We also thank the U.S. Forest Service and the Colorado Geological Survey for their cooperation. Reviews by Werner Aeschbach-Hertig, Peter McMahon, and Bert Stolp were very helpful and improved the manuscript.

References

- Aeschbach-Hertig, W., P. Schlosser, M. Stute, H. J. Simpson, A. Ludin, and J. F. Clark (1998), A $^3\text{H}/^3\text{He}$ study of ground water flow in a fractured bedrock aquifer, *Ground Water*, *36*, 661–670.
- Aeschbach-Hertig, W., F. Peeters, U. Beyerle, and R. Kipfer (1999), Interpretation of dissolved atmospheric noble gases in natural waters, *Water Resour. Res.*, *35*, 2779–2792.
- Aeschbach-Hertig, W., F. Peeters, U. Beyerle, and R. Kipfer (2000), Paleotemperature reconstruction from noble gases in ground water taking into account equilibration with entrapped air, *Nature*, *405*, 1040–1043.
- Ballentine, C. J., and C. M. Hall (1999), Determining paleotemperature and other variables by using an error-weighted, nonlinear inversion of noble gas concentrations in water, *Geochim. Cosmochim. Acta*, *63*, 2315–2336.
- Bayer, R., P. Schlosser, G. Bönisch, H. Rupp, F. Zaucker, and G. Zimmek (1989), Performance and blank components of a mass spectrometric system for routine measurement of helium isotopes and tritium by the ^3He ingrowth method, in *Sitzungsberichte der Heidelberger Akademie der Wissenschaften, Mathematisch-Naturwissenschaftliche Klasse*, vol. 5, pp. 241–279, Springer, New York.
- Birch, F. (1950), Flow of heat in the Front Range, Colorado, *Geol. Soc. Am. Bull.*, *61*, 567–630.
- Bossong, C. R., J. S. Caine, D. I. Stannard, J. L. Flynn, M. R. Stevens, and J. S. Heiny-Dash (2003), Hydrologic conditions and assessment of water resources in the Turkey Creek Watershed, Jefferson County, Colorado, 1998–2001, *U.S. Geol. Surv. Water Resour. Invest. Rep.*, *03-4034*, 140 pp.
- Bredehoeft, J. D., and I. S. Papadopoulos (1965), Rates of vertical groundwater movement estimated from the Earth's thermal profile, *Water Resour. Res.*, *1*, 325–328.
- Burns, D. A., P. S. Murdoch, G. B. Lawrence, and R. L. Michel (1998), Effect of groundwater springs on NO_3^- concentrations during summer in Catskill Mountain streams, *Water Resour. Res.*, *34*, 1987–1996.
- Caine, J. S., and S. R. A. Tomasiak (2003), Brittle structures and their role in controlling porosity and permeability in a complex Precambrian crystalline-rock aquifer system in the Colorado Rocky Mountain Front Range, *Geol. Soc. Am. Bull.*, *115*, 1410–1424.
- Caine, J. S., A. H. Manning, P. L. Verplanck, D. J. Bove, K. G. Kahn, and S. Ge (2006), Well construction information, lithologic logs, water level data, and overview of research in Handcart Gulch, Colorado: An alpine watershed affected by metalliferous hydrothermal alteration, *U.S. Geol. Surv. Open File Rep.*, *06-1189*, 14 pp.
- Cook, P. G., and J. K. Böhlke (2000), Determining timescales for groundwater flow and solute transport, in *Environmental Tracers in Subsurface Hydrology*, edited by P. G. Cook and A. L. Herczeg, pp. 1–30, Springer, New York.
- Cook, P. G., A. J. Love, N. I. Robinson, and C. T. Simmons (2005), Groundwater ages in fractured rock aquifers, *J. Hydrol.*, *308*, 284–301.
- Decker, E. R. (1969), Heat flow in Colorado and New Mexico, *J. Geophys. Res.*, *74*, 550–559.
- Dekay, R. H. (1972), Development of ground-water supplies in Shenandoah National Park, Virginia, *Rep. 10*, Va. Div. of Miner. Resour., Charlottesville.
- Desbarats, A. J. (2002), A lumped-parameter model of groundwater influx to a mine adit in mountainous terrain, *Water Resour. Res.*, *38*(11), 1256, doi:10.1029/2001WR001058.
- Diersch, H.-J. D. (1998), *FEFLOW: Reference manual—Release 4.7*, WASY, Berlin.
- Domenico, P. A., and V. V. Palciauskas (1973), Theoretical analysis of forced convective heat transfer in regional ground-water flow, *Geol. Soc. Am. Bull.*, *84*, 3803–3814.
- Ferguson, G., H. Beltrami, and A. D. Woodbury (2006), Perturbation of ground surface temperature reconstructions by groundwater flow?, *Geophys. Res. Lett.*, *33*, L13708, doi:10.1029/2006GL026634.
- Forster, C., and L. Smith (1989), The influence of groundwater flow on thermal regimes in mountainous terrain: A model study, *J. Geophys. Res.*, *94*, 9439–9451.
- Guan, H. (2005), Water above the mountain front—Assessing mountain-block recharge in semiarid regions, Ph.D. thesis, N. M. Inst. of Mining and Technol., Socorro.
- Haitjema, H. M. (1995), On the residence time distribution in idealized groundwatersheds, *J. Hydrol.*, *172*, 127–146.
- Heaton, T. H. E., and J. C. Vogel (1981), “Excess air” in groundwater, *J. Hydrol.*, *50*, 201–216.
- Hely, A. G., R. W. Mower, and C. A. Harr (1971), Water resources of Salt Lake County, Utah, *Tech. Publ. 31*, Utah Dep. of Nat. Resour., Salt Lake City.
- Herrmann, A., and W. Stichler (1980), Groundwater-runoff relationships, *Catena*, *7*, 251–264.
- Holoher, J., V. Matta, W. Aeschbach-Hertig, U. Beyerle, M. Hofer, F. Peeters, and R. Kipfer (2001), Noble gas and major element constraints on the water dynamics in an alpine floodplain, *Ground Water*, *39*, 841–852.
- International Atomic Energy Agency (2006), Isotope Hydrology Section database, Vienna. (Available at <http://isohis.iaea.org>)
- Johnson, R. H., L. Wirt, R. R. McDougal, A. H. Manning, D. B. Yager, D. L. Fey, and K. J. Leib (2007), Geochemistry of surface and ground water in Cement Creek from Gladstone to Georgia Gulch and in Prospect Gulch, San Juan County, Colorado, *U.S. Geol. Surv. Open File Rep.*, *07-1004*.
- Kahn, K. G. (2005), Analysis of the shallow groundwater system in an alpine basin: Handcart Gulch, Colorado, M.S. thesis, 148 pp., Univ. of Colo., Boulder.
- Kimball, B. A., R. L. Runkel, and L. J. Gerner (2001), Quantification of mine drainage inflows to Little Cottonwood Creek, Utah, using a tracer-injection and synoptic-sampling study, *Environ. Geol.*, *40*, 1390–1404.
- Kimball, B. A., R. L. Runkel, K. Walton-Day, and K. Bencala (2002), Assessment of metal loads in watersheds affected by acid mine drainage by using tracer injection and synoptic sampling: Cement Creek, Colorado, USA, *Appl. Geochem.*, *17*, 1183–1207.
- Kipfer, R., W. Aeschbach-Hertig, F. Peeters, and M. Stute (2002), Noble gases in lakes and ground waters, in *Reviews in Mineralogy and Geochemistry*, vol. 47, *Noble Gases in Geochemistry and Cosmochemistry*, edited by D. Porcelli et al., pp. 615–700, Mineral. Soc. of Am., Chantilly, Va.
- Kosugi, K., S. Katsura, M. Katsuyama, and T. Mizuyama (2006), Water flow processes in weathered granitic bedrock and their effects on runoff generation in a small headwater catchment, *Water Resour. Res.*, *42*, W02414, doi:10.1029/2005WR004275.

- Liu, F., M. W. Williams, and N. Caine (2004), Source waters and flow paths in an alpine catchment, Colorado Front Range, United States, *Water Resour. Res.*, 40, W09401, doi:10.1029/2004WR003076.
- Lovering, T. S. (1935), Geology and ore deposits of the Montezuma Quadrangle, Colorado, *U.S. Geol. Surv. Prof. Pap.*, 178, 119 pp.
- Maloszewski, P., and A. Zuber (1982), Determining the turnover time of groundwater systems with the aid of environmental tracers: 1. Models and their applicability, *J. Hydrol.*, 57, 207–231.
- Maloszewski, P., W. Rauert, W. Stichler, and A. Herrmann (1983), Application of flow models in an alpine catchment area using tritium and deuterium data, *J. Hydrol.*, 66, 319–330.
- Manning, A. H., and D. K. Solomon (2004), Constraining mountain-block recharge to the Eastern Salt Lake Valley, Utah, with dissolved noble gas and tritium data, in *Groundwater Recharge in a Desert Environment: The Southwestern United States*, *Water Sci. Appl. Ser.*, vol. 9, edited by J. F. Hogan et al., pp. 139–158, AGU, Washington, D. C.
- Manning, A. H., and D. K. Solomon (2005), An integrated environmental tracer approach to characterizing groundwater circulation in mountain block, *Water Resour. Res.*, 41, W12412, doi:10.1029/2005WR004178.
- Manning, A. H., D. K. Solomon, and A. L. Sheldon (2003), Applications of a total dissolved gas pressure probe in ground water studies, *Ground Water*, 41, 440–448.
- Manning, A. H., D. K. Solomon, and S. A. Thiros (2005), $^3\text{H}/^3\text{He}$ age data in assessing the susceptibility of wells to contamination, *Ground Water*, 43, 353–367.
- Maréchal, J. C. (1999), Observation des massifs cristallins alpins au travers des ouvrages souterrains: 2. Définition du rôle hydrogéologique de la zone décomprimée, *Hydrogéologie*, 2, 33–42.
- Maréchal, J. C., and D. Etcheverry (2003), The use of ^3H and ^{18}O tracers to characterize water inflows in Alpine tunnels, *Appl. Geochem.*, 18, 339–351.
- Mau, D. P., and T. C. Winter (1997), Estimating ground-water recharge and baseflow from streamflow hydrographs for a small watershed in New Hampshire, *Ground Water*, 35, 291–304.
- Mayo, A. L., and W. Koontz (2000), Fracture flow and groundwater compartmentalization in the Rollins Sandstone, Lower Mesaverde Group, Colorado, USA, *Hydrogeol. J.*, 8, 430–446.
- Mayo, A. L., T. H. Morris, S. Peltier, E. C. Petersen, K. Payne, L. S. Holman, D. Tingey, T. Fogel, B. J. Black, and T. D. Gibbs (2003), Active and inactive groundwater flow systems: Evidence from a stratified, mountainous terrain, *Geol. Soc. Am. Bull.*, 115, 1456–1472.
- Mazor, E., R. O. van Everdingen, and H. R. Krouse (1983), Noble-gas evidence for geothermal activity in a karstic terrain: Rocky Mountains, Canada, *Geochim. Cosmochim. Acta*, 47, 1111–1115.
- Mendoza, G. F., T. S. Steenhuis, M. T. Walter, and J. Y. Parlange (2003), Estimating basin-wide hydraulic parameters of a semi-arid mountainous watershed by recession-flow analysis, *J. Hydrol.*, 279, 57–69.
- Mulholland, P. J. (1993), Hydrometric and stream chemistry evidence of three storm flowpaths in Walker Branch Watershed, *J. Hydrol.*, 151, 291–316.
- Plummer, L. N., E. Busenberg, J. K. Bohlke, D. L. Nelms, R. L. Michel, and P. Schlosser (2001), Groundwater residence times in Shenandoah National Park, Blue Ridge Mountains, Virginia, USA: A multi-tracer approach, *Chem. Geol.*, 179, 93–111.
- Polyakov, V. A., S. A. Medvedev, and N. V. Pyatnitskij (1996), An isotopic and hydrochemical study of the groundwater inflow into the north-Muya tunnel, in *Isotopes in Water Resource Management: Proceedings of a Symposium on Water Resources Management*, Int. At. Energy Agency, Vienna.
- Rademacher, L. K., J. F. Clark, G. B. Hudson, D. C. Erman, and N. A. Erman (2001), Chemical evolution of shallow groundwater as recorded by springs, Sagehen basin, Nevada County, California, *Chem. Geol.*, 179, 37–51.
- Rademacher, L. K., J. F. Clark, and J. R. Boles (2003), Groundwater residence times and flow paths in fractured rock determined using environmental tracers in the Mission Tunnel, Santa Barbara County, California, USA, *Environ. Geol.*, 43, 557–567.
- Rahn, P. H. (1981), Ground water stored in the rocks of western South Dakota, in *Geology of the Black Hills, South Dakota and Wyoming, Field Trip Guide Book*, Geological Society of America, edited by F. J. Rich, pp. 154–173, Am. Geol. Inst., Alexandria, Va.
- Rauber, D., H. H. Loosli, H. Schmassmann, and J. N. Andrews (1991), Noble gases in groundwater, in *Applied Isotope Hydrogeology: A Case Study in Northern Switzerland*, *Stud. Environ. Sci. Ser.*, vol. 43, edited by F. J. Pearson et al., pp. 117–149, Elsevier, New York.
- Robinson, C. S. (1978), Hydrology of fractured crystalline rocks, Henderson Mine, Colorado, *Min. Eng.*, 30, 1185–1194.
- Robinson, C. S., F. T. Lee, J. H. Scott, R. D. Carroll, R. T. Hurr, D. B. Richards, F. A. Mattei, B. E. Hartmann, and J. F. Abel (1974), Engineering geologic, geophysical, hydrologic and rock-mechanics investigations of the Straight Creek Tunnel site and pilot bore, Colorado, *U.S. Geol. Surv. Prof. Pap.*, 815, 134 pp.
- Runkel, R. L., B. A. Kimball, K. Walton-Day, and P. L. Verplanck (2003), When good tracers go bad: Tracer-dilution sausage recipes revealed, *Eos Trans. AGU*, 84(46), Fall Meet. Suppl., Abstract H51C-1044.
- Sanford, W. E., R. G. Shropshire, and D. K. Solomon (1996), Dissolved gas tracers in groundwater: Simplified injection, sampling, and analysis, *Water Resour. Res.*, 32, 1635–1642.
- Schlosser, P., M. Stute, H. Dorr, C. Sonntag, and K. O. Munnich (1988), Tritium/ ^3He dating of shallow groundwater, *Earth Planet. Sci. Lett.*, 89, 353–362.
- Schlosser, P., M. Stute, C. Sonntag, and K. O. Munnich (1989), Tritogenic ^3He in shallow groundwater, *Earth Planet. Sci. Lett.*, 94, 245–256.
- Snow, D. T. (1973), Mountain groundwater supplies, *Mountain Geol.*, 10, 19–24.
- Solomon, D. K. (2000), ^4He in groundwater, in *Environmental Tracers in Subsurface Hydrology*, edited by P. G. Cook and A. L. Herczeg, pp. 425–439, Springer, New York.
- Soulsby, C., R. Malcolm, and I. Malcolm (2000), Groundwater in headwaters: Hydrological and ecological significance, *Geol. Soc. Spec. Publ.*, 182, 19–34.
- Stute, M. and P. Schlosser (2000), Atmospheric noble gases, in *Environmental Tracers in Subsurface Hydrology*, edited by P. G. Cook and A. L. Herczeg, pp. 349–377, Springer, New York.
- Stute, M., M. Forster, H. Frischkorn, A. Serejo, J. F. Clark, P. Schlosser, W. S. Broecker, and G. Bonani (1995), Cooling of tropical Brazil (5°C) during the Last Glacial Maximum, *Science*, 269, 379–383.
- Stute, M., J. Deak, K. Revesz, J. K. Bohlke, E. Deseeoe, R. Weppernig, and P. Schlosser (1997), Tritium/ ^3He dating of river infiltration: An example from the Danube in the Szigetkoz area, Hungary, *Ground Water*, 35, 905–911.
- Sueker, J., J. N. Ryan, C. Kendall, and R. D. Jarrett (2000), Determination of hydrologic pathways during snowmelt for alpine/subalpine basins, Rocky Mountain National Park, Colorado, *Water Resour. Res.*, 36, 63–75.
- Tiedeman, C. R., D. J. Goode, and P. A. Hsieh (1998), Characterizing a ground water basin in a New England mountain and valley terrain, *Ground Water*, 36, 611–620.
- Todd, A., and D. McKnight (2003), Abandoned mines, mountain sports, and climate variability: Implications for the Colorado tourism economy, *Eos Trans. AGU*, 84(38), 377386.
- Uhlenbrook, S., M. Frey, C. Leibundgut, and P. Maloszewski (2002), Hydrograph separations in a mesoscale mountainous basin at event and seasonal timescales, *Water Resour. Res.*, 38(6), 1096, doi:10.1029/2001WR000938.
- VanderBeek, G. A. (2003), Estimating recharge and storage coefficient in a fractured rock aquifer, Turkey Creek Basin, Jefferson County, Colorado, M.S. thesis, 115 pp., Colo. School of Mines, Golden.
- Vogel, J. C. (1967), Investigation of groundwater flow with radiocarbon, in *Isotopes in Hydrology, Rep. IAEA-SM-83/7*, pp. 355–369, Int. At. Energy Agency, Vienna.
- Wasiolka, M. (1995), Subsurface recharge to the Tesuque Aquifer system from selected drainage basins along the western side of the Sangre de Cristo Mountains near Santa Fe, New Mexico, *U.S. Geol. Surv. Water Resour. Invest. Rep.*, 94–4072, 57 pp.
- Wilson, J. L., and H. Guan (2004), Mountain-block hydrology and mountain-front recharge, in *Groundwater Recharge in a Desert Environment: The Southwestern United States*, *Water Sci. Appl. Ser.*, vol. 9, edited by J. F. Hogan et al., pp. 113–137, AGU, Washington, D. C.
- Wilson, G. B., and G. W. McNeill (1997), Noble gas recharge temperatures and the excess air component, *Appl. Geochem.*, 12, 747–762.
- Zecharias, Y. B., and W. Brutsaert (1988), Recession characteristics of groundwater outflow and baseflow from mountainous watersheds, *Water Resour. Res.*, 24, 1651–1658.
- Zuber, A., S. M. Weise, K. Osenbruck, J. Grabczak, and W. Cieczkowski (1995), Age and recharge area of thermal waters in Ladek Spa (Sudeten, Poland) deduced from environmental isotope and noble gas data, *J. Hydrol.*, 167, 327–349.